Treatise on the Meteorological Aspects of the TMI-2 Accident

continued (Part II)

by Ignaz Vergeiner, Ph. D.

February 1995

Table of contents

Treatise on the Meteorological Aspects of the TMI-2 Accident

continued (Part II)

by Ignaz Vergeiner, Ph. D.

1. Introduction

In my "Treatise on the TMI-2 Accident of March 28, 1979, particularly its meteorological aspects including transport and dispersion of the radionuclides released" finished at the end of June 1994 I have presented and interpreted the general weather pattern accompanying the first few days after the TMI-2 partial core melt on March 28, 1979. Characteristic features are very strong elevated inversions and generally weak and changeable winds, conducive to stagnation. I have pursued the inferences on regional and local patterns of flow and dispersion of radionuclides released around the TMI plant. Over and above a critique of the Defendants' Gaussian modelling procedures, I have presented and argued my own scenarios and quantitative estimates of how very highly concentrated plumes or puffs could have inflicted very high doses to people, animals and plants locally along some of the hill slopes, up to tens and even hundreds of rems, as opposed to the tens or hundreds of millirems claimed by the Defendants.

I fully uphold my analyses in this June 1994 treatise, from now on called "Part I". Part II offers an opportunity to expand on my earlier results.
New model calculations will also be presented (chapter 6), and visualization of transport processes at work will be provided by shallow-water laboratory experiments at the University of Karlsruhe (chapter 7).

I will present a calendar of meteorological events, starting before "time zero" on March 28, 1979, 04 E.S.T., and leading up to March 29, 06 E.S.T. A somewhat longer time span of 3 days had been considered in part I - the more limited time span addressed now in considerably more detail reflects the still prevalent conclusion that the largest releases occurred on the very first day.

I wish to reiterate the points made in the introduction to part I. Although the meteorological analysis stands on its own, the determination of the overall course of events still resembles solving a puzzle. Very few usable hard facts have been provided by GPU and the official agencies involved, particularly for the first, all-important day. What little there is, is from the near vicinity of TMI.

Even if the Defendants had been prepared and willing to dedicate all personnel and instruments available to following the plumes and puffs emanating from TMI-2, they could not possibly have covered all the hill sites and slopes exposed to such releases, even to five or ten miles, much less beyond. This fact makes it mandatory to consider the biological evidence as primary evidence. There were no instruments out there, but there were people and trees, for example, very effectively serving as instruments or, to put it more bluntly, as unintentional "guinea pigs". This body of evidence can provide verification of the transport and dispersion models, and provide sound scientific methodology to confirm the location and magnitude of accident releases of radioactivity.

The limited data base, beginning with highly unsatisfactory official data on times, composition and quantity of releases, carrying on to plume and puff concentrations across a very complex hilly countryside being modeled with necessarily limited consideration of the extreme meteorological conditions, all serve to emphasize the point that, rather than pursuing only single strands of evidence, it is necessary to establish the coherence of an overall pattern by as much cross-checking as possible.

2. The general weather situation revisited

2.1 Notation

Time will be Eastern Standard Time throughout.
Although, for example, 12 Greenwich Time (UTC) = 07 E.S.T., the 06 E.S.T. weather observations are combined with the 12 UTC soundings, as the balloons are usually launched one hour ahead of nominal time 12 or 00 UTC. 28/06 will be March 28, 1979, 06 E.S.T. = 06 a. m.

Actual temperature may come either in ° C or in ° F. For conversion see figs. 2.2.

It was explained in part I why a fictitious quantity called "potential temperature" Θ is most useful when comparing temperatures at various elevations.

To within a degree C or so,

Θ in degrees Kelvin $\approx$
$\approx$ actual temperature (°C) + elevation MSL (meters)/100 - 2 (2.1)

for our purposes.

When and where the atmosphere is well-mixed, Θ = constant with height, for example on a sunny day around noon from the surface up to the height of the "mixing layer" (see figs. 2.2 and 3.4).
In this case, actual temperature, by equ. (2.1), decreases by 1 °C per 100 m elevation ("adiabatic lapse rate"). In general, Θ cannot decrease with height. The faster Θ increases with height, the more "STABLE" the particular atmospheric layer is said to be.

Air pressure p is expressed in millibars (mb) or, equivalently, hectopascals (hPa). Reference must be made to part I. For one, pressure can be used as an alternative height scale. For example, the pressure level 850 mb could lie anywhere between, say, 1100 m and 1800 m a.s.l. Its mean height ("STANDARD ATMOSPHERE") is taken to be 1457 m. In our case (relatively high pressure), its height is $\approx$ 1500 to 1560 m.

Inasmuch small pressure differences across a horizontal surface ("pressure gradients") are being considered, this is conveniently done in terms of a quantity called DP - see chapter 4.2.

Wind direction is given on a 360 ° scale:

90 ° wind from the east
180 ° wind from the south
270 ° wind from the west
360 ° wind from the north.

Wind speed is alternately expressed in

mph = statute miles per hour

or

kn = knots = nautical miles per hour

or

m/s = meters per second.

This may be awkward, but a radical unification of units was deemed impractical.

1 mph = 0,447 m/s
1 kn = 0,515 m/s.

2.2 Illustrating some weather elements

As shown in detail in part I, time zero of the TMI-2 disaster = March 28, 1979, 04 E.S.T. very nearly coincided with the passage of a high-pressure ridge followed by vigorous warm-air advection from the southwest. Within three days temperatures up to 500 mb rose by almost 20 ° C, which is clearly seen in figs. 2.2. For later reference, the airport stations used in the further analyses are entered on the map fig. 2.1. Pittsburgh and Washington D. C. are radiosonde stations as well, the third one considered here, Albany, N. Y., does not fit on this map (see figs. 5.3 and following).

The massive frontal inversion is evident in figs. 2.2, approaching the area under consideration and lowering accordingly. Upper winds are generally from westerly directions, whereas winds in the lower layers turn from northerly (cold-air advection) to southerly (warm-air advection).

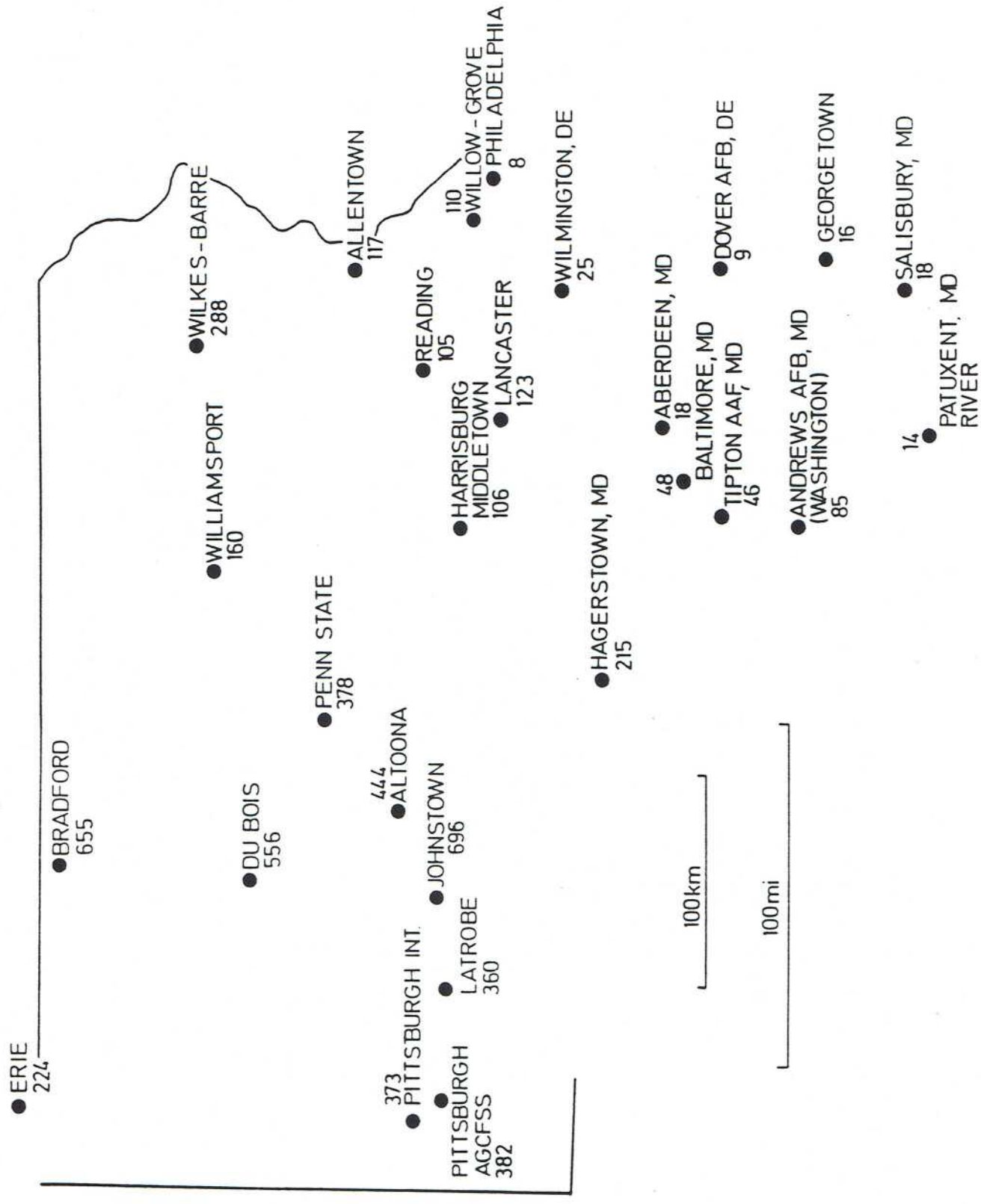

Fig. 2.1: *Airport stations used, Pennsylvania, Maryland and Delaware, with elevations in m MSL.*

Figs 2.2:

Soundings at Pittsburgh (a), Albany, N. Y. (b) and Washington, D.C. (c) for indicated dates. 28/07 = March 28, 1979, 07 E.S.T.

Temperatures are actual temperatures, not potential temperatures, with a Fahrenheit scale added at the bottom.

Height in m MSL on the right is approximate, except for station height.

$\Gamma_{ADIABAT}$ is the "adiabatic" temperature lapse rate – 1 °C/100 m at perfect mixing.

Winds for the first four dates (27/19 to 29/07) drawn on the left.

Wind from SSE, 10 knots

Wind from WNW, 25 knots

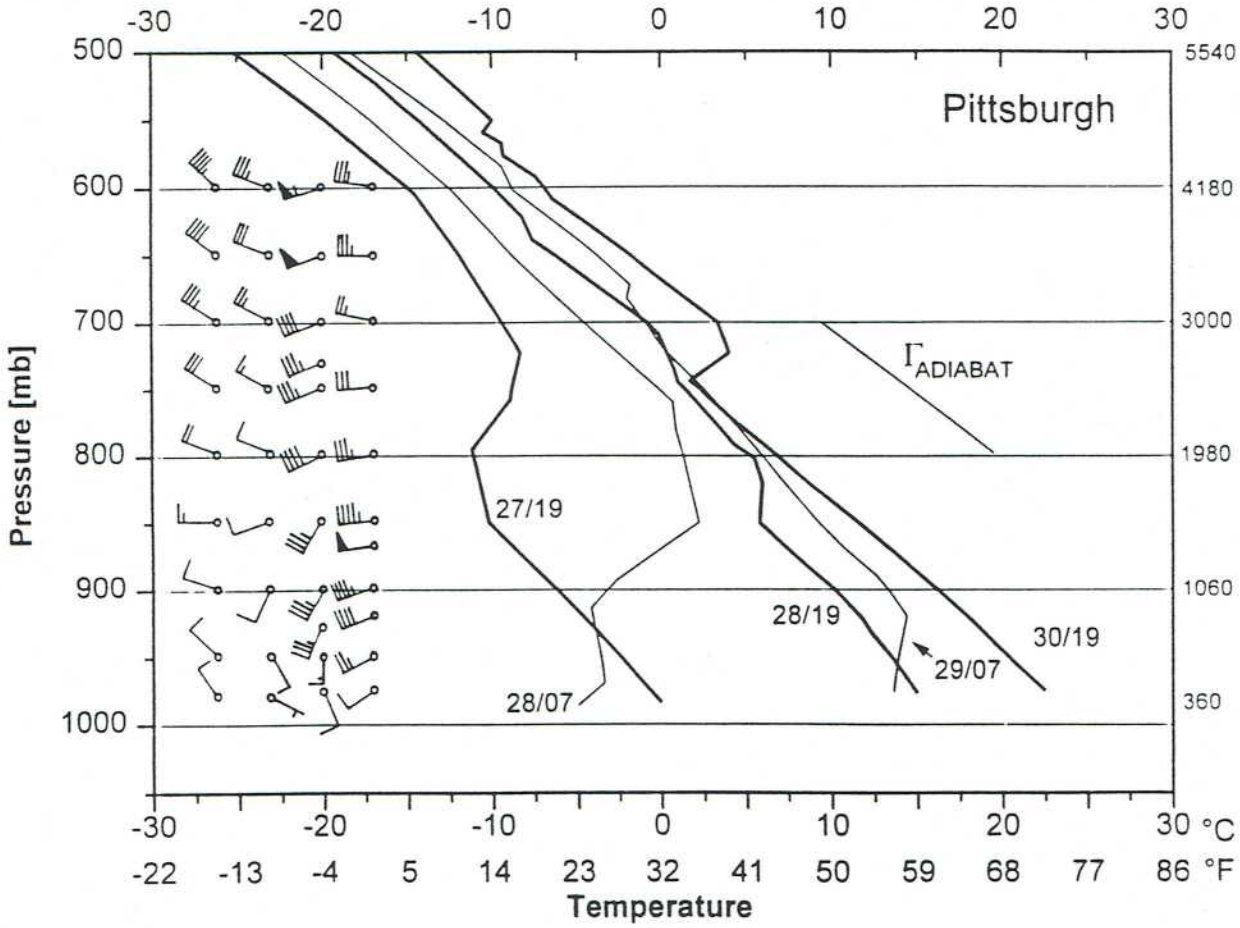

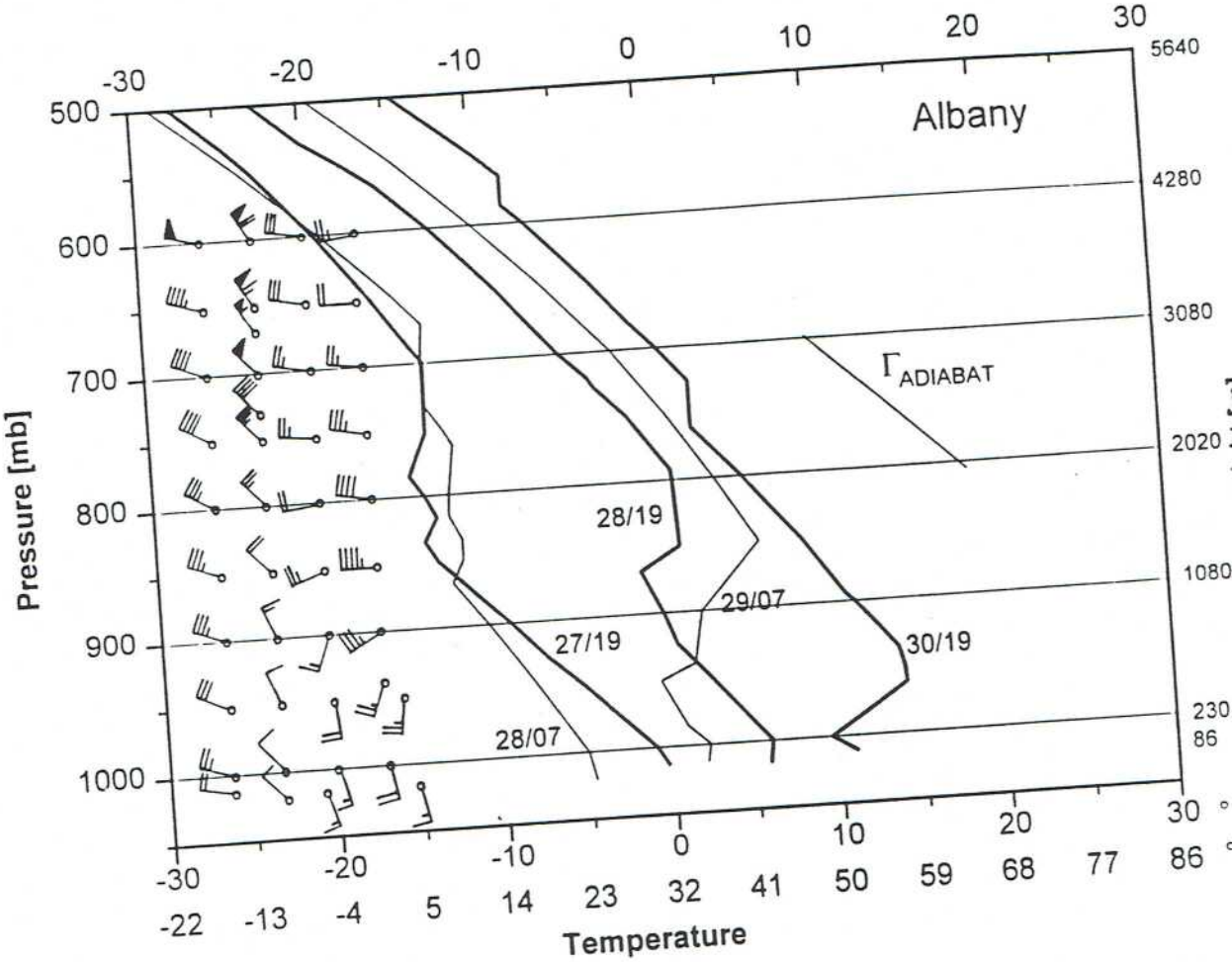
Albany
Pressure [mb]
Temperature
$\Gamma_{ADIABAT}$
28/19
29/07
27/19
30/19
28/07
500
600
700
800
900
1000
-30
-20
-10
0
10
20
30
-22
-13
-4
5
14
23
32
41
50
59
68
77
86
5640
4280
3080
2020
1080
230

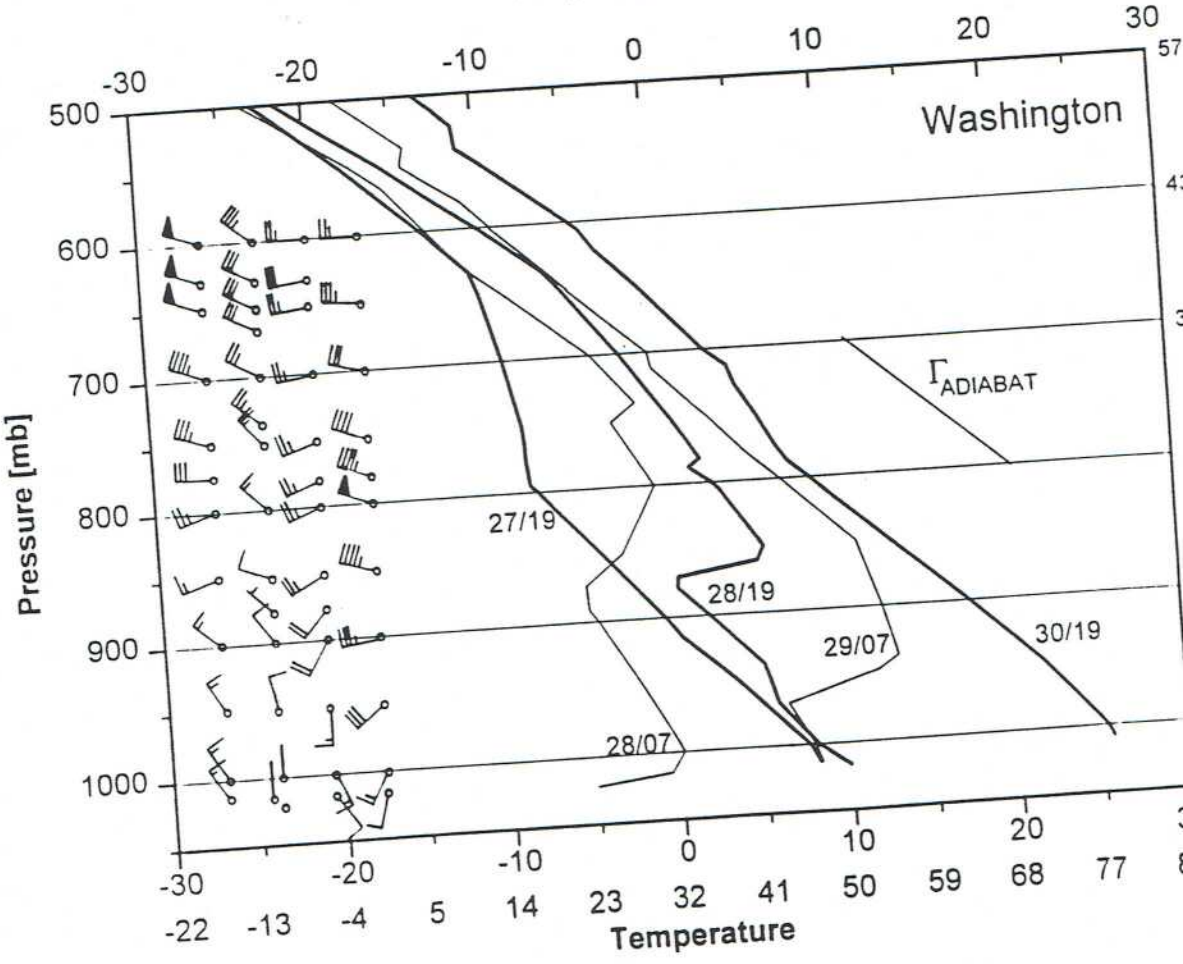
Washington
Pressure [mb]
Temperature
$\Gamma_{ADIABAT}$
27/19
28/19
29/07
30/19
28/07
500
600
700
800
900
1000
-30
-20
-10
0
10
20
30
-22
-13
-4
5
14
23
32
41
50
59
68
77

Albany is consistently colder than Washington and Pittsburgh, but the temperature contrast weakens in the course of March 28/29. Figs. 2.2 display the massive general warming in the course of the three days 27/19 to 30/19 very well, amounting to more than 15 ° C. The simultaneous moistening of the atmosphere can be inferred from the little table in chapter 4.1.

Another way to illustrate the course of events is plotting the march of (actual) temperature and dew point temperature for selected stations (figs. 2.3) and the march of air pressure at those same stations (figs. 2.4). Looking at the station temperatures first, the daily march of temperature (daytime heating, nighttime cooling) is clearly seen on all three days, superimposed by the massive general advective warming.

The dew point temperature is a unique function of the air's water vapor content, as long as we stay in the same altitude range. Therefore, it is a good airmass indicator. On a quiet, sunny day, the water vapor mixing ratio might drop by ≈ 10 or 20 percent around noon because of mixing with drier air on top, but otherwise it stays fairly constant. The pronounced rise of the dew point here accompanies the moistening of the boundary layer, as the warm air advected from the Gulf of Mexico is also very moist air.

The march of air pressure (figs. 2.4) is mainly a dramatic reflection of the warm air advection and concomitant pressure fall in advance of the cyclonic system approaching from the west. The pressure fall is considerably more dramatic on the western side of the Appalachians. Quasi-diurnal pressure signals reflecting the daytime heating (warmer air is lighter) and nighttime cooling (colder air is heavier) are much less evident here. This is to be expected, as air pressure at any level equals the weight of the air column above that level (hydrostatic law), and is therefore an integral measure, to which the surface layer contributes less than the "free atmosphere" above. Also, the daily march of pressure contains signals from tidal waves, which do not change local horizontal or vertical gradients, but tend to obscure the relatively small signals from boundary layer heating or cooling.

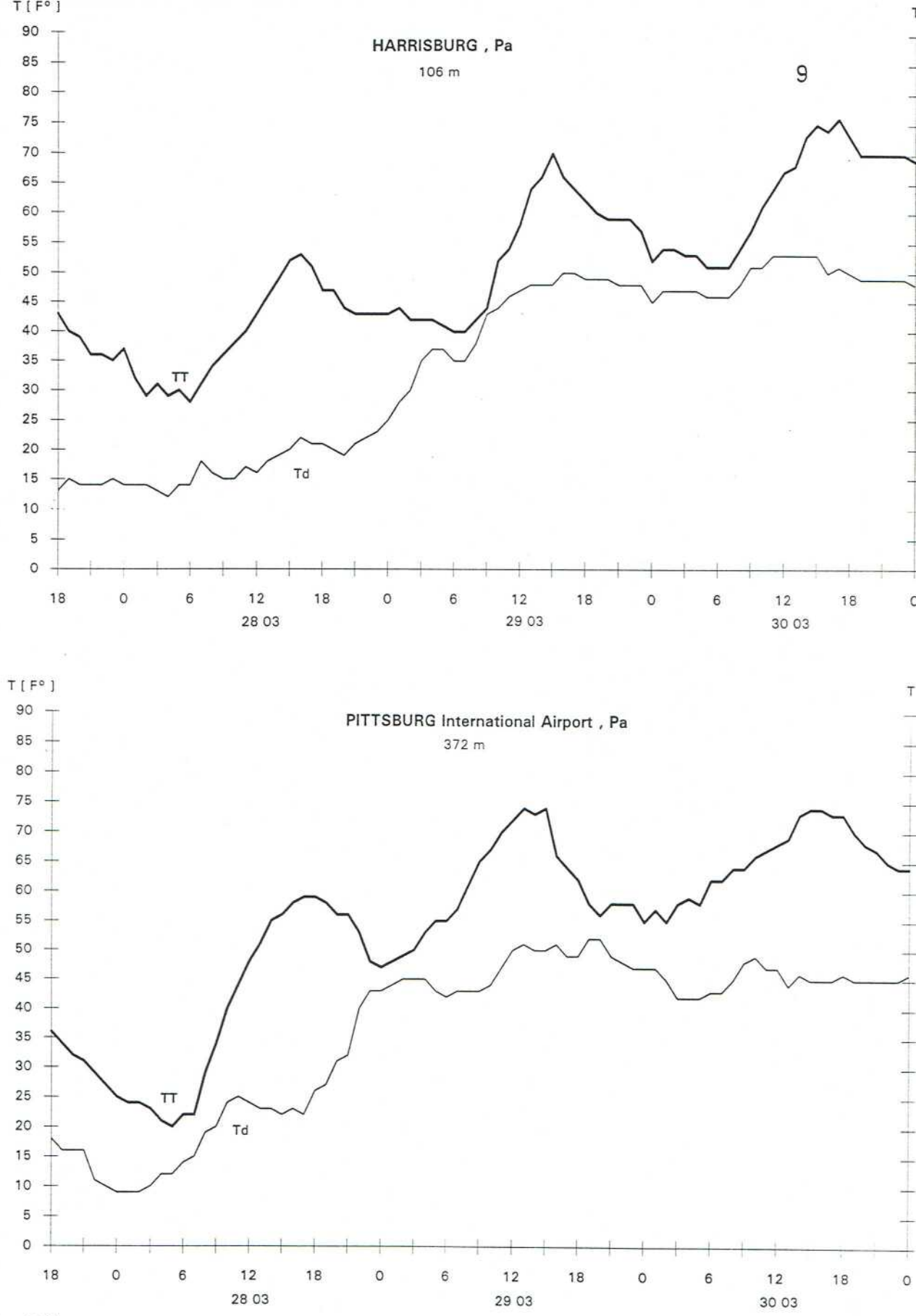

Fig. 2.3:
Course of station temperature (TT) and dew point temperature (Td) in °F at indicated stations between the evening of March 27 and March 30, 1979.

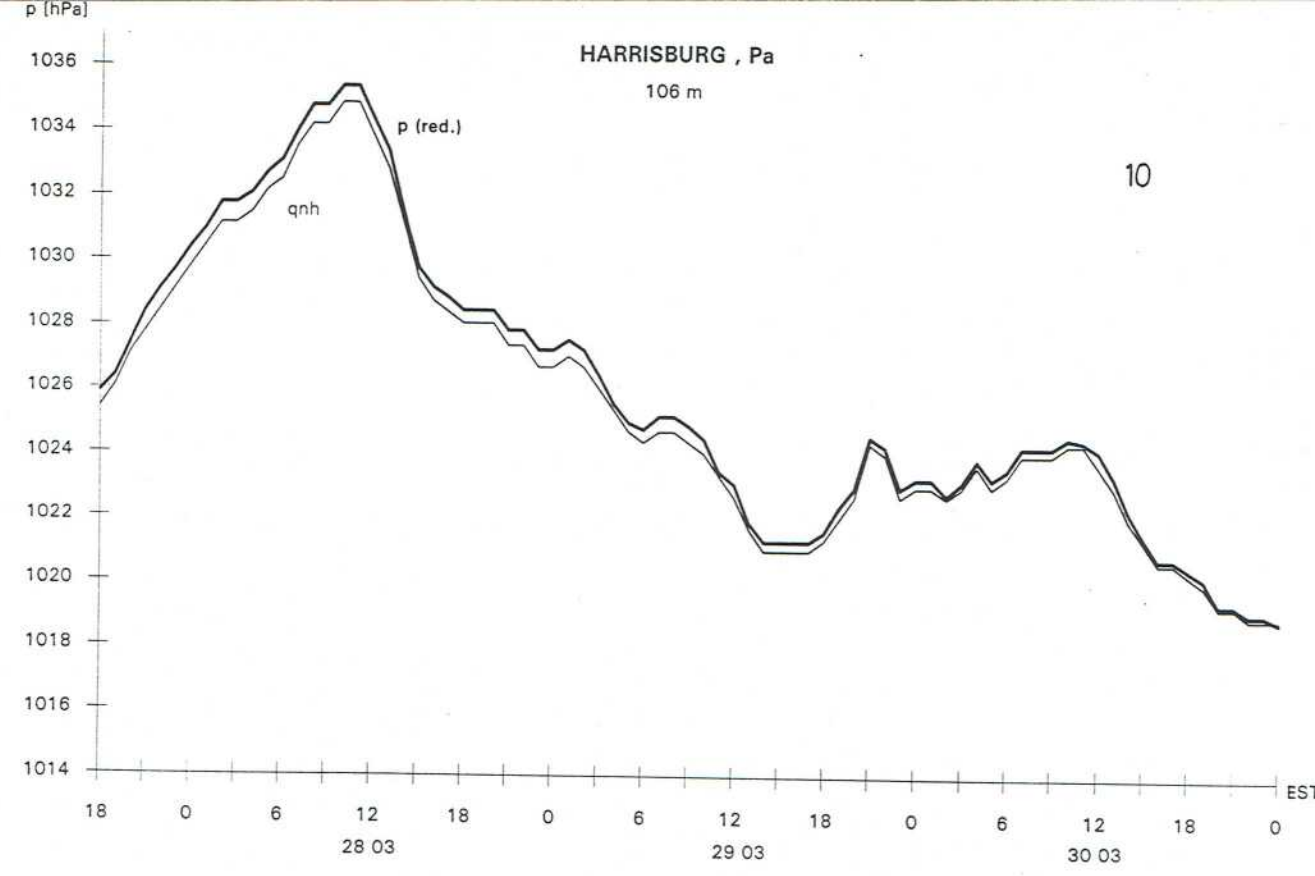

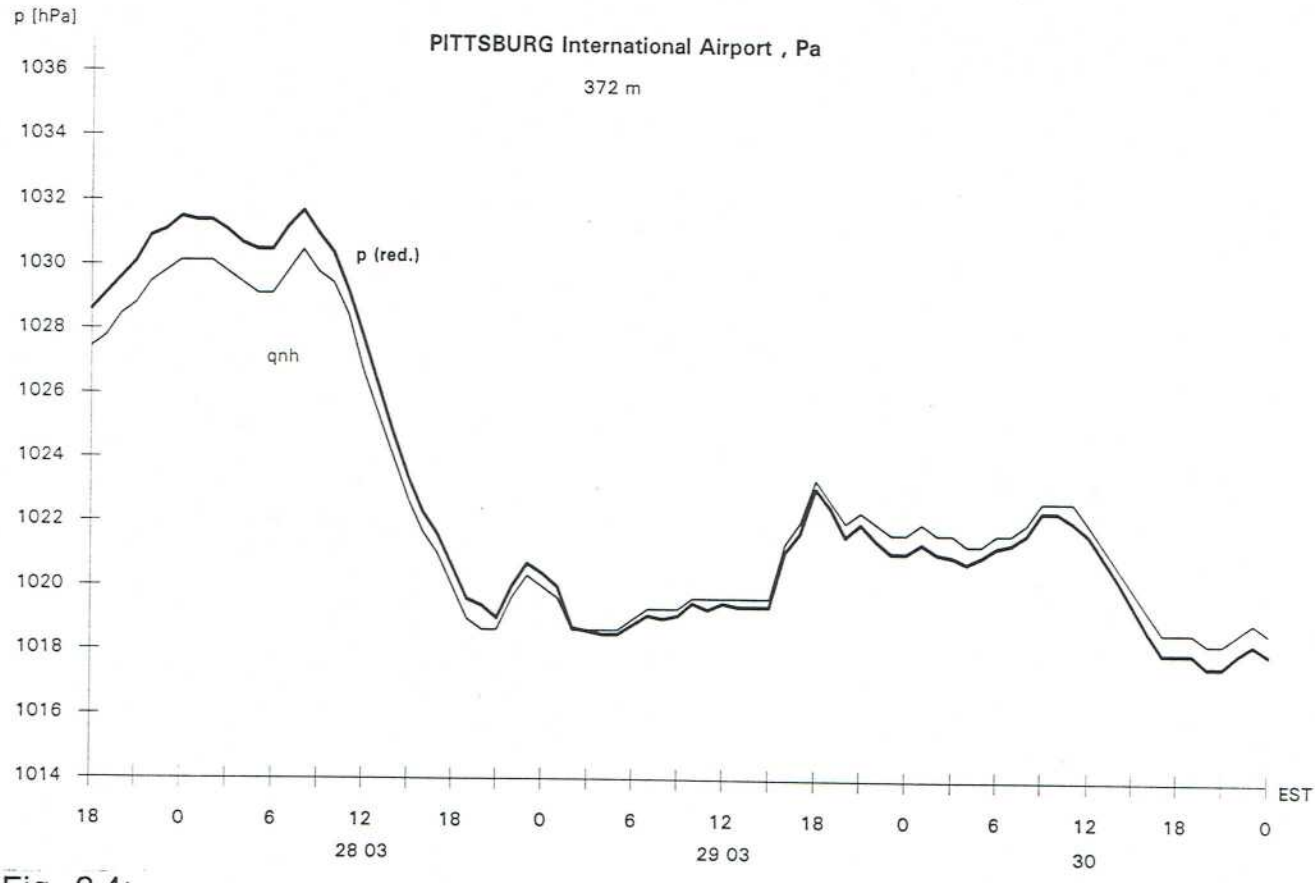

Fig. 2.4:

Course of pressure, reduced to sea level, in hPa = mb for stations and time span as in fig. 2.3.
Thick line: Pressure reduction using station temperature
Thin line: Pressure reduction using standard atmosphere (QNH = altimeter setting)

3. Synoptic forcing versus local daytime/nighttime influence

The gist of this chapter is to show that although in our case the "synoptically forced" temperature, pressure and wind patterns induced by the travelling highs and lows are substantially stronger than the respective patterns caused by solar daytime heating and by nighttime cooling of the earth's surface including the Appalachian hill slopes, we must not ignore the latter influence of the "thermal boundary layer", as these changes occur very near the surface, inducing characteristic low-level temperature and wind features highly significant for transport and dispersion of pollutants which are no more than a few hundred feet above ground.

The synoptic course of events, treated in detail in part I, will only be given a quick rerun here. The broad frontal zone has a wavy flow pattern shown schematically in fig. 3.1, which may be visualized to propagate as a whole (not quite unchanged, of course) from west to east at a speed of roughly 30 mph.

The surface high passed the Harrisburg area at or slightly after 4 a. m., time zero of the TMI-2 disaster, the upper ridge at about 9 a. m. Thereafter, the new cyclone approaching from the west started strong warm-air advection and accompanying surface pressure fall by early afternoon of March 28. This pressure fall amounted to ≈ 6 or 8 mb on March 28 across eastern Pennsylvania, and up to ≈ 10 mb across the Northwest Plateau on this very first day alone (see figs 2.4). Surges of colder and warmer air are linked to these synoptic pressure patterns. Ahead of a first warm front pressure gradients strengthen both at upper levels and at the surface. Light rains fall in the early morning hours of March 29 (roughly 0.04 inch total), while the formidable frontal inversion descends and surface pressure gradients weaken again across Eastern Pennsylvania as a consequence of enforced stagnation.

Local influence of daytime heating and nighttime cooling

A word on the data situation is in order here. Whereas the network of airport stations is sufficient for resolving the synoptic-scale processes, the location and density of stations precludes any attempt to find thermal pressure or flow features on the local scale, whether they be mechanically or thermally forced. In particular, the Appalachian slopes to the near west of the Harrisburg area are not covered by any station at all. Therefore, I take guidance from studies on slope winds and valley winds in the Alps and Bavarian foreland, and related studies

Fig. 3.1: *Wavy synoptic pattern, schematic*

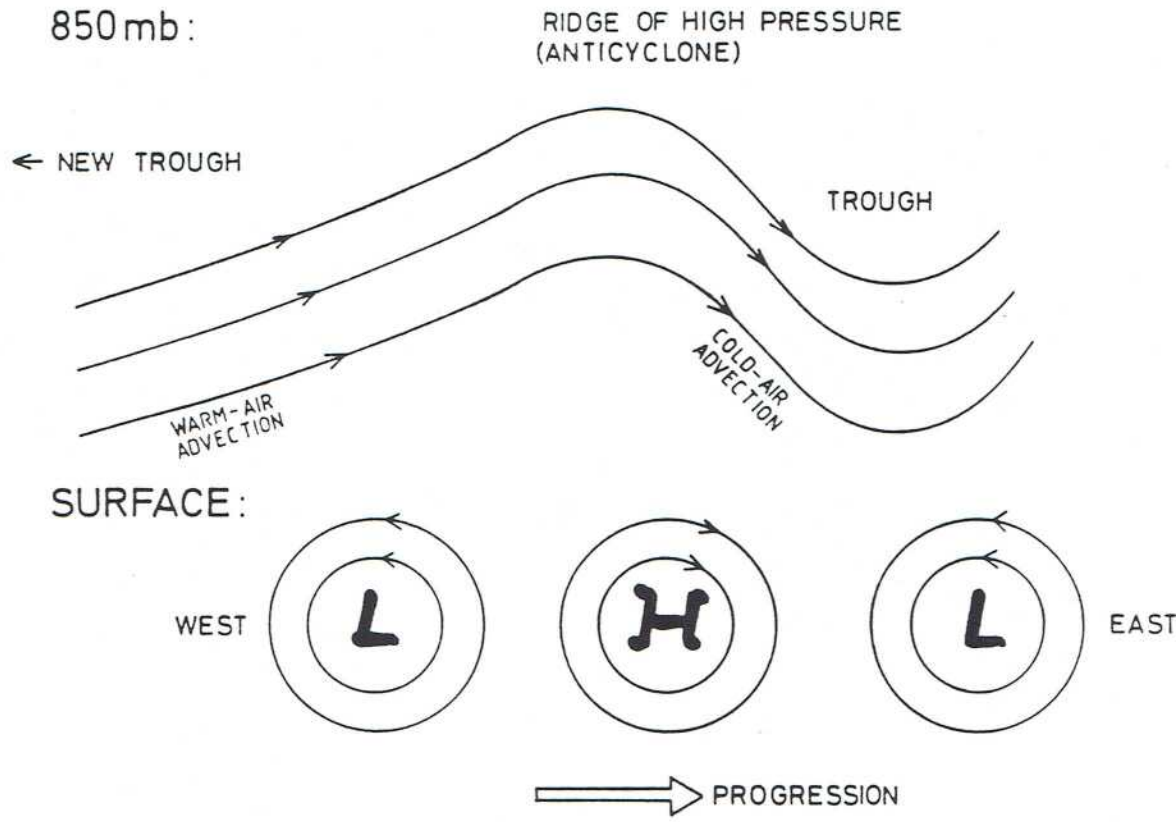

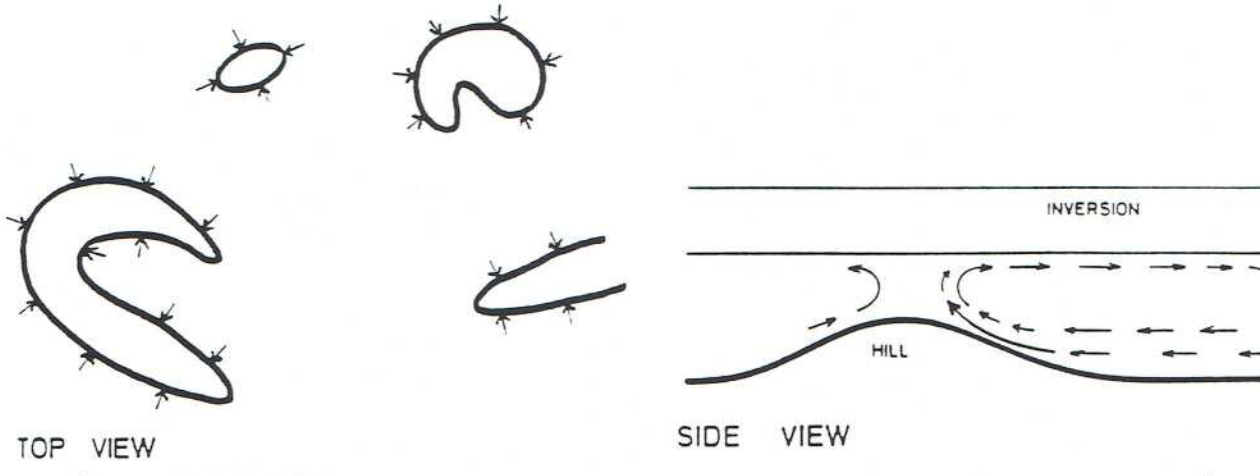

Fig. 3.2:
Slope wind circulations, schematic
Top view (lower or middle part of hills) and side view.

on Colorado valleys and in other parts of the Western US, taking due account of the considerably gentler slopes of the Appalachian hills. For my own contributions to this field, see Vergeiner (1982), Vergeiner and Dreiseitl (1987) and Vergeiner, Dreiseitl and Whiteman (1987). For summaries of the state of observations and theory on these matters, see chapters 2 and 3 in Blumen (1990) by Whiteman and Egger.

The processes described further down are best seen in conditions of weak synoptic gradients, like e. g. during the early and late morning hours after time Zero on March 28. This does not mean that thermal forcing does not act in "windier" conditions, too, but then its effects will be harder to recognize because they will be "overridden" by the synoptic gradients.

If the countryside was strictly a plain, daytime solar heating and nighttime cooling by long-wave radiation would act on the adjacent air layers only from below, from the earth's surface upward. Daytime mixed layers and nighttime inversions will form according to rather well-established principles (see e. g. the very shallow 5 ° C inversion at Washington D. C., shown on the sounding of March 28/06 E.S.T. in fig. 2.2c, and the decaying phase of a mixed layer ≈ 1200 m deep 12 hours later, same figure). Mixed layers and inversions will still form over hilly or mountainous countryside, but now there are substantial modifications, as the mountain slopes form elevated sources of heating and cooling. 20 minutes or half an hour after sunrise upslope breezes will develop when and where the sun hits a slope. They are very localized like thermal plumes, concentrated in ravines, missing on ridges, reacting almost instantly to sunshine or shadow, between a few m and, say, 100 m deep, with speeds hardly reaching 1 m/s. They should not be thought of as steady air currents, but in the ensemble they constitute very many small-scale thermal circulations schematically shown in figs. 3.2 and 3.3. There is a quasi-horizontal inflow towards the hill necessary to feed the thin upslope layer, and a return flow preferably beneath an inversion. Obviously, with many dispersed hills of varying shapes and heights the circulations may become extremely chaotic in detail, but their net effect will always be to induce subsiding air motions over the valleys and ravines between the hills and over the foreland adjacent to the mountains.

These subsiding motions, small as they are in the range of cm/s, serve to communicate the heating along the slope surface to the free atmosphere over the foreland, in addition to the direct heating from below out there. Incidentally, they also stabilize the atmospheric layer

Fig. 3.3:
Slope wind circulations, schematic.
Side view with Appalachians.
a) Late morning time like 10 a. m.

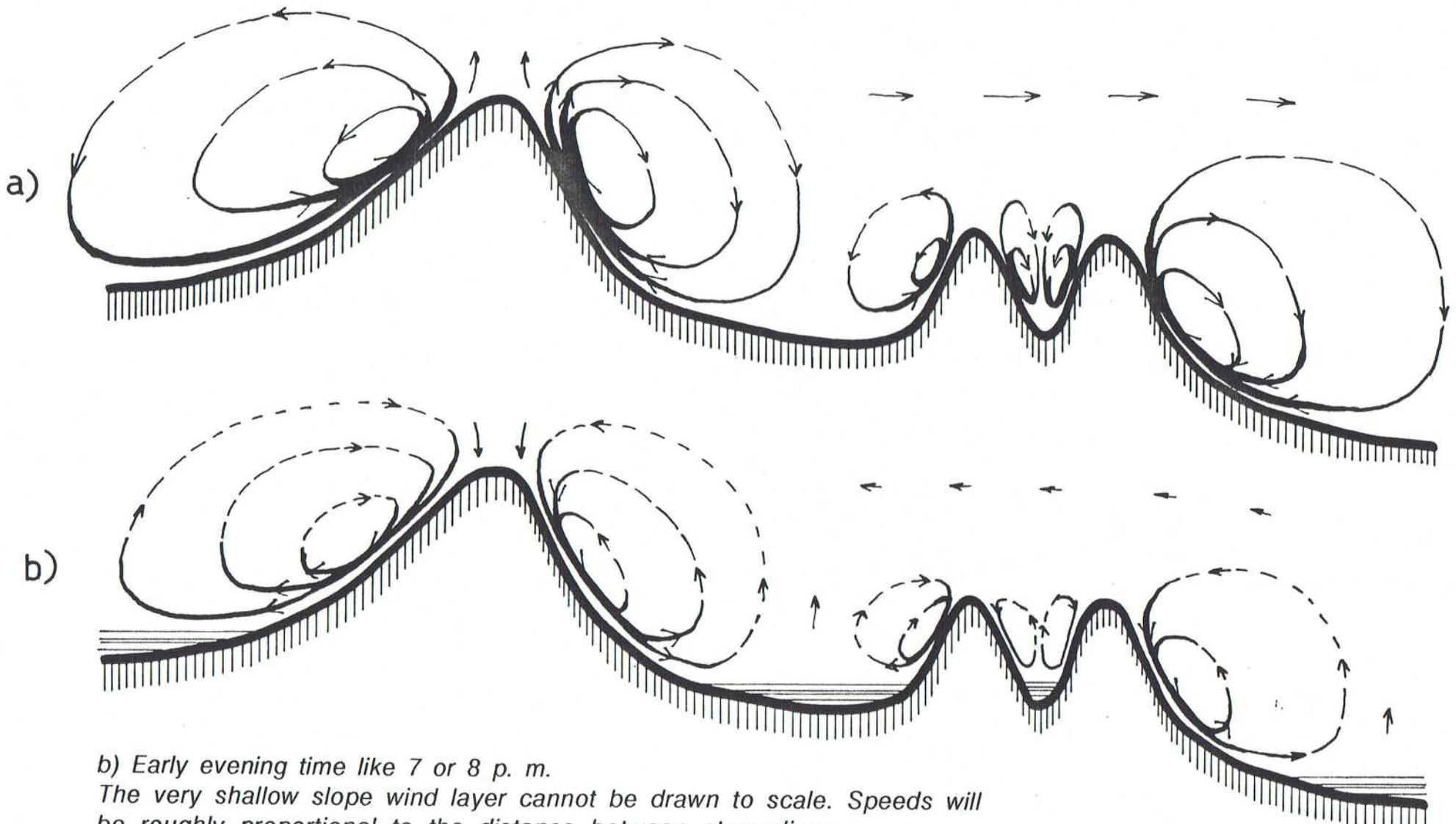

b) Early evening time like 7 or 8 p. m.
The very shallow slope wind layer cannot be drawn to scale. Speeds will be roughly proportional to the distance between streamlines.

affected, thereby retarding the growth of the mixed layer and suppressing turbulence. In recent numerical simulations, Lu and Turco (1994) have very nicely shown thermal upslope circulations with return currents beneath an inversion and subsidence away from the mountains, albeit in a quite different setting including a sea-breeze circulation. In our case, the cool Susquehanna river at ≈ 7 ° C will strengthen the thermal contrast to the heated slopes and, therefore, strengthen the daytime ensemble of circulations described above.

The nighttime situation with cooling of the slopes has, by and large, reversed circulations: "katabatic" downslope flows, accumulating cold pockets of air in valleys, basins and other sheltered, low-lying areas.

An attempt to vizualize the circulation patterns schematically is shown in figs. 3.3 for two times of the day. The height of an inversion or more inversions will be an important parameter in determining the precise vertical structure of the slope-wind circulation systems. Horizontal inflow speeds in the daytime will be weak, reaching on the order of a m/s only where there is some flow channeling, but that is sufficient to slowly "suck in" radioactive plumes or puffs hanging around in the morning hours towards the hill slopes. That would be mostly westward, but occasionally in other directions as well, depending on the hill's location and shape.

The overall thermal state of the atmosphere in a cross section across the Appalachians, taking account of observed or derived vertical temperature profiles from the Pittsburgh and Washington radiosondes, would show the frontal inversion near 850 mb, and the presumed local features at low levels, in line with the foregoing discussion of upslope and downslope circulations. The overall pattern gets complicated further by a most characteristic thermal plateau effect:
Both daytime heating and nighttime cooling will usually be quite similar across eastern or western Pennsylvania, but this thermal input occurs at two different elevations, ≈ 100 m and ≈ 380 m MSL, respectively, with some parts of the NW plateau up to 600 m and more.

Resuming the topic of the Alps or similarly high and steep mountains once more, with long valleys cut deep into the mountain relief, there we have not only slope winds, but a rather well-developed quasi-periodic upvalley and downvalley wind regime: These winds transporting many millions of m^3/s follow along-valley pressure gradients, the upvalley winds starting in the late morning, a few hours after sunrise, and reversing in the evening, some hours after sunset. It turns out that these valley winds owe their existence to the fact that mainly for

geometric reasons the mass of air to be heated or cooled in a valley is so much less compared to a plain that the daily range of vertical mean temperature in an Alpine valley is ≈ 2.2 times that over the adjacent plain. Consequently, the thermally induced pressure fall in major Alpine valleys may reach 6 mb or so.

Whereas slope winds in the Appalachians are expected to develop collectively much like in the Alps, the situation is different with respect to valley winds. The "area-height distribution" (see Steinacker, 1984) of the Appalachians will be shrunk to about 1/3 the height range of a typical Alpine valley region, and their gentler valleys are not as well sheltered against outside intervention by synoptic pressure gradients and winds as the deep Alpine valleys. In other words, by Alpine standards, Appalachian valleys are no real valleys! But again, they are quite sufficient for upslope and downslope circulations, including e. g. cold-air pooling.

I have no data on hand on valley winds in the Appalachians, but according to the best of my knowledge I assume that they will resemble more "slope winds along the valley floor", that typical speeds will be more like 1 to 3 m/s rather than the 5 to 10 m/s often observed in the Alps, and that their reaction time will be more like one or two hours (after sunrise) rather than ≈ 4 hours or so in Alpine valleys. There is a further problem with the extremely confusing relief of Appalachian valleys: How should we imagine the sum total of upvalley winds up the Susquehanna river valley heading north plus many other valleys heading west or southwest? In essence, I assume that Appalachian valleys will have a tendency to channel what are essentially slope winds, that a corresponding "upvalley" wind mixture between southerly and easterly will develop around, say, 7 or 8 E.S.T. in the Harrisburg and TMI area, a couple of 100 m deep and at ≈ 1 - 3 m/s when fully developed around noon, but that this wind system will be overruled by the synoptic winds from the southsoutheast when they begin to pick up speed around noon. It is a matter of speculation whether downvalley winds from the north or northwest could have continued for a little while at heights of several dekameters a. g. even after a shallow upslope layer had begun to form near the valley floor around 7 a. m. Such sandwiching of opposing wind currents has been observed (e. g. see Whiteman, 1990).

Finally, let us pursue the quantitative implication of daytime heating for the evolving vertical temperature profiles. A reasonable estimate for the sensible heat input H at this time of year is:

6	7	8	9	10	11	12	13	14	15	16h	local time
30	50	80	110	140	150	130	100	50	10		W/m^2

Starting out with a given vertical profile of temperature T (or potential temperature Θ) at, say, 06 h, this heat flux serves to warm the air close to the ground such that a layer of increasing depth becomes mixed (Θ = const or $\partial T/\partial z = -1$ ° C/100 m) - see fig. 3.4 a.
For simplicity, I have assumed here, in agreement with the foregoing considerations on valley winds, that the "topographic amplification factor" is not far different from 1, i. e. the value over a plain. It can be shown then that the stippled area in fig. 3.4 a representing the total heating in a given time δt (in hours)

$$\int \delta T \text{ (°C)} \cdot dz \text{ (m)} \approx 3 \cdot \overline{H} \text{ (W/m}^2\text{)} \cdot \delta t \text{ (h)}$$

Evaluating this expression with the values for sensible heat flux H given above, the area representing the heating will be

06 - 09 h	09 - 12 h	12 - 15 h	local time
$\overline{\delta T} \cdot \Delta z = 500$	1200	850	°C.m
or $\overline{\delta T} \cdot \Delta p = 50$	120	85	°C.mb with 100 mb ≈ 1000 m.

Using the hydrostatic law, this translates into a pressure fall of altogether hardly more than 1 mb, confirming again the predominance of synoptic forcing at upper levels. Close to the ground, however, the shape of the vertical temperature profile, and thereby static stability and flow and dispersion properties, do depend on local heating and cooling.
Incidentally, the change of temperature profiles at Albany and Pittsburgh between March 28, 06 E.S.T. (observed) and 09 E.S.T. (derived), shown in fig. 3.4 b appears to confirm the above estimates, although the superimposed large synoptic change (subsidence/advection) makes it rather difficult to isolate the local effect. At Albany, with a less stable sounding, the same heating $\overline{\delta T} \cdot \Delta p$ will cause a deeper mixed layer than at Pittsburgh with its extremely stable sounding.

The above ideas will be used, among others, in reconstructing the gross features of the presumed vertical temperature profiles at Harrisburg - see chapters 4 and 5.

Fig. 3.4:

a) Morning inversion, schematic, successively dissolved by heating from the surface, forming a shallow mixed layer. Temperature scale is potential temperature Θ.

b) Actual soundings, March 28, 1979, 06 and 09 E.S.T., Albany, N.Y. (solid lines) and Pittsburgh (dashed lines).

Temperature scale is potential temperature Θ.

06 E.S.T.: from actual sounding

09 E.S.T.: derived (see chapter 4).

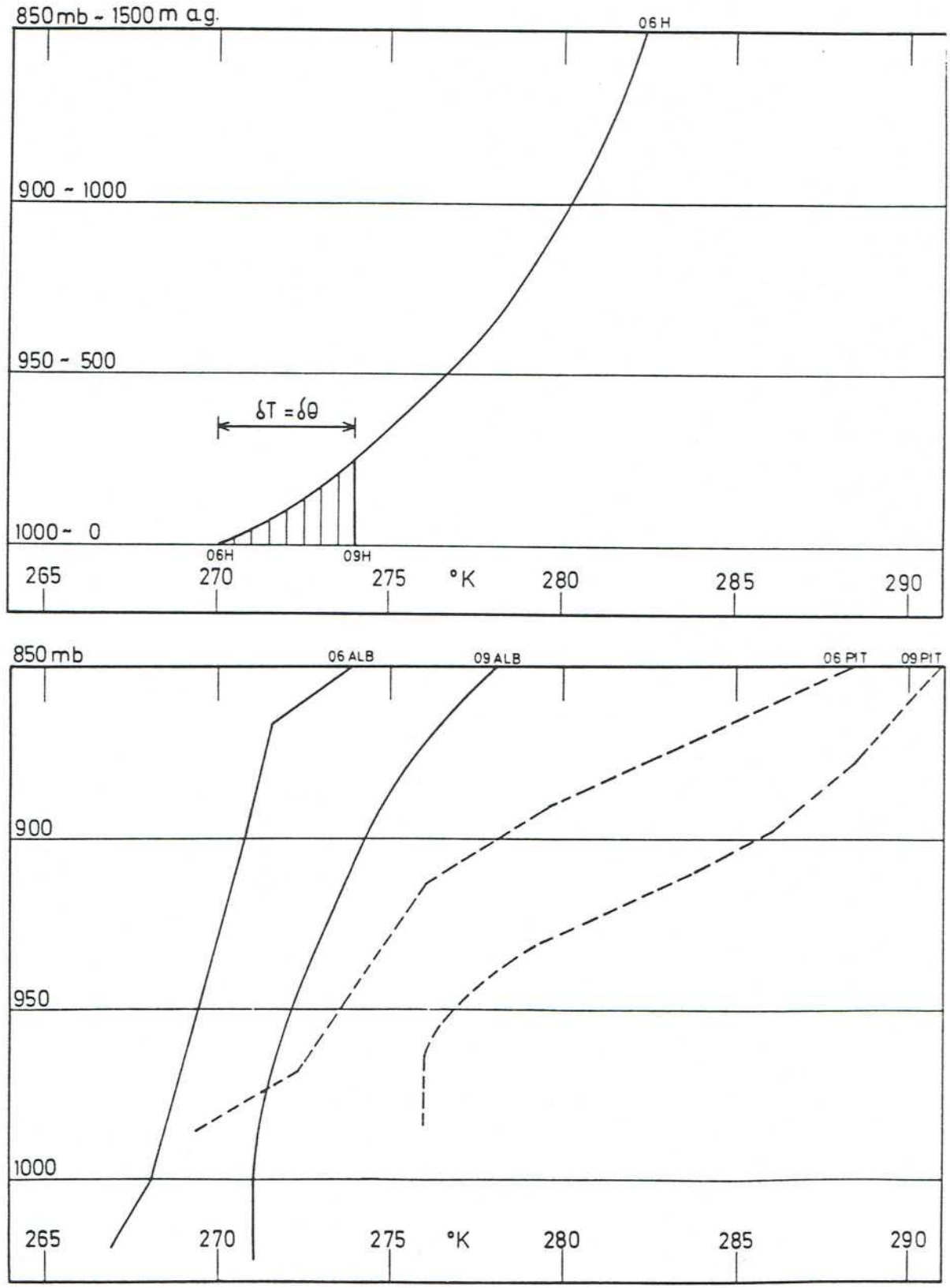

4. Techniques for Data Evaluation and Interpolation

4.1 Upper air data

Our only probes of the atmosphere away from the surface are the radiosoundings at 12 hour intervals. It was explained in part I how better resolution in time can be attained by drawing isolines of potential temperature on time-height sections: The results for Pittsburgh, Albany, N. Y., and Washington D. C. were plotted there in figs 2.7 a, b, c.

The main idea is to bridge the gap between the frequent surface measurements and the 12-hourly interval at upper levels, assuming that upper-level features change more smoothly than surface features.

Starting out with surface pressure available from many stations (see 4.3) including, of course, the radiosonde stations, we can now compute pressure (or height) at upper levels hydrostatically, using the temperature profiles derived above for the three radiosonde stations. A suitable form of the hydrostatic equation to start with is

$$\Delta H = - \frac{29{,}27}{0{,}2857} \overline{\Theta}_v \cdot \Delta \left(\frac{p}{1000} \right)^{0{,}2857} \qquad (4.1)$$

Here p is pressure in mb,
H is height in m,
Δ denotes the difference between two levels
and $\overline{\Theta_v}$ is the mean virtual potential temperature of the layer between the two levels in deg K.

"Virtual" temperature must be used in hydrostatic computations rather than temperature, in order to account for the moisture content of air:

$$\Theta_v = \Theta \cdot (1 + 0.61 \cdot 10^{-3} q), \qquad (4.2)$$

where q = grams of water vapor per kilograms of air.

The difference is a couple of degrees at most. In our case, it turns out that the correction term may be approximated to be the same across the region of interest, and roughly constant from the surface up to 850 mb as follows:

	28. III.								29. III.			
	00	03	06	09	12	15	18	21	00	03	06	EST
$\Theta_v - \Theta \approx$	0.4	0.4	0.4	0.4	0.5	0.5	0.5	0.6	0.8	0.9	1.0	°K

Actually, instead of the contour height H of a given pressure surface p I work with a quantity called DP. A short presentation of this technique will be deferred to chapter 4.2. The proper adaptation of equ. (4.1) will be given there.

In any case, however, derived contour heights of the 850 mb surface are now available every 3 hours, say, at the three sounding sites. These three values, by themselves, would not suffice to draw approximate 850 mb contour maps at intermediate time intervals. Only a linear field could be interpolated from them. Remember, however, that we have some knowledge of the wavy synoptic pattern with its progression of ridges and troughs (see fig. 3.1) and that at least every 12 hours reasonably accurate contour maps can be drawn by using not only contour heights, but also gradients of the contour height, assuming geostrophic flow and taking observed winds. Official NMC analyses including observations from New York and Buffalo were also consulted. In the end, a sequence of three-hourly 850 mb contour maps has been produced, shown in chapter 5 figs. 5.3, 5.4 a and following. To the extent to which these smooth fields are a good approximation, they yield spatial resolution as well as timewise resolution several times superior to the original upper-air sounding data.

In combination with the abundant surface pressure data (chapter 4.3), mean potential temperatures $\overline{\Theta}$ may now be computed for the layer between 850 mb and the surface at this same spatial and timewise resolution by applying equ. (4.1) or its adapted forms (4.6), and subtracting the "virtual difference" (Θ_V - Θ) as quoted above. In chapter 5, this vertical average $\overline{\Theta}$ will be used to demonstrate a last surge of cold-air advection across eastern Pennsylvania in the mid-morning of March 28. More generally, this average $\overline{\Theta}$ taken together with the bounding values Θ (surface) and Θ (850 mb) (see below), with an understanding of local heating and cooling effects (see chapter 3) and with guidance from the 12-hourly observed temperature profiles at the three sounding stations and their time-interpolated values (part I, figs. 2.7 a, b, c) permits reconstructing the gross features of the vertical

temperature profile at each location, not only the sounding sites. The result will be presented for Harrisburg only in fig. 5.2.

The technique for deriving an approximate field of Θ at 850 mb at improved spacewise and timewise resolution is largely analogous to the one shown earlier for contour height H or DP, respectively.
Theoretically, the thermal wind relation might be used to obtain horizontal gradients of Θ from the vertical wind shear $\partial V/\partial z$ observed in the soundings, but this is impractical in this highly inhomogeneous temperature field with a strong frontal inversion near the 850 mb-level. Starting out with the three point values of Θ (850 mb) (part I, figs. 2.7 a, b, c) and linear interpolation in between, this first guess is modified by consideration of the wavy synoptic pattern of temperature, and of the front and rear end of the first warm front at 850 mb as shown on the much-quoted time-height-sections of Θ.

4.2 Working with DP instead of contour height H

This technique has been advanced by Bellamy (1945) and Steinacker et al. (1987), among others.

DP is defined as

$$DP = H - H_{ST}(p), \tag{4.3}$$

where H = height of a station or a pressure surface
and H_{ST} (p) = height of that same pressure surface
(observed station pressure = p)
in the "STANDARD ATMOSPHERE".

The mathematical definition of the STANDARD ATMOSPHERE will not be repeated here. Essentially, it is a convenient reference atmosphere with sea-level pressure = 1013,25 mb, sea-level temperature t_v = 15 °C = 288 °K and with temperature decreasing with height at the rate of 0.65 °C per 100 m up to the tropopause.

If we stay on a pressure surface p = const., it is immediately obvious that DP behaves exactly like the contour height H. For example, H_{ST} (850 mb) = 1457 m, and contour maps of the 850 mb-surface may be relabelled to yield maps of DP in meters by subtracting out 1457 m.

In the same spirit, assuming geostrophic equilibrium to apply above the boundary layer (which may be not too good an assumption at 850 mb in our case due to the frontal inversion)

$$u_g = \frac{-g}{f} \cdot \frac{\partial}{\partial y} DP$$

$$v_g = \frac{+g}{f} \cdot \frac{\partial}{\partial x} DP \qquad (4.4)$$

where (x, y) are Cartesian coordinates pointing east and north,
(u_g, v_g) are the corresponding wind components
(geostrophic wind presumably ≈ actual wind),
g is 9,81 ms^{-2} and f is the Coriolis parameter ≈ $0.95 \cdot 10^{-4}$ s^{-1}.

The real advantage of preferring DP over H comes from comparing values along the vertical. By subtracting out the standard atmosphere, the resulting DP is a number not exceeding, say, +/- a couple of 100 meters, and becomes amenable to easy comparison and interpolation along the vertical. More specifically, DP-values are related to temperatures hydrostatically via the pertinent form of the hydrostatic equation

$$\frac{\partial DP}{\partial z} = \frac{T_v(p) - T_{vST}(p)}{T_v(p)} \qquad (4.5)$$

where $\frac{\partial DP}{\partial z}$ = change of DP along height z,

T_v (p) = actual (virtual) temperature and

T_{vST} (p) = (virtual) temperature of Standard Atmosphere, both at pressure p.

In other words, DP = constant with height where the atmospheric layer is at standard temperature, DP increases with height where the atmosphere is warmer than standard, and DP decreases with height where the atmosphere is colder than the standard atmosphere.

For example, a cold surface high beneath an upper trough would have positive DP (relatively "high pressure") at the surface, decreasing

upward and turning negative ("low pressure") at upper levels. Yet another way of applying the hydrostatic equation between two pressure levels, say 850 and 980 mb, is to use equ. (4.1) first, obtaining

$$\Delta H = 4.059\ \overline{\Theta_v}\ ,$$

and then to note the definitions of DP (equ. 4.3):

$$DP_{850} = H\ (850) - 1457\ m$$
$$DP_{980} = H\ (980) - 281\ m$$

wherefrom $DP_{850} - DP_{980} = \Delta H - 1176\ m,$

or $DP_{850} - DP_{980} = 4.059\ \overline{\Theta_V} - 1176\ m = 4.059\ (\overline{\Theta_V} - 289.8).$

Here, $\overline{\Theta_V}$ is the mean virtual potential temperature (see further up) for the layer between 850 and 980 mb.

A series of analogous relations may be derived; some are noted down here for later use:

$$DP_{850} = DP_{950} + 3.158 * (\overline{\Theta_V} - 290.4)$$

$$DP_{850} = DP_{980} + 4.059 * (\overline{\Theta_V} - 289.8) \qquad (4.6)$$

$$DP_{850} = DP_{1012} + 4.998 * (\overline{\Theta_V} - 289.5)$$

1012 mb, incidentally, is approximately taken to be the elevation 100 m MSL or a convenient reference level for Eastern Pennsylvania ("surface"), as opposed to the Western Plateau (≈ 980 mb) or the Northwest (see fig. 2.1, ≈ 950 mb).

4.3. Surface data

Little needs to be said about surface temperature.
Conversion of actual temperatures to potential temperatures was noted already in chapter 2.1. Actually, the exact definition

$$\Theta = T \cdot \left(\frac{1000}{p}\right)^{0.2857}, \qquad T = t\ (°C) + 273.15$$

was used here rather than the approximation, as pressure p is available at all stations. Slight inconsistencies or nonrepresentative values, like e. g. the very low morning temperature at Washington (fig. 2.2 c), when no other surrounding station shows it, have been ironed out. Of course, this does not mean that the surface temperature depressed by 5 °C beneath that strong surface inversion has not been measured correctly! Only that local phenomena need to be taken into account separately.

Pressure needs some special treatment.
All stations report "altimeter setting" or QNH, which is pressure reduced to sea level using the (fictitious) standard atmosphere. Some stations also report the conventional "surface pressure" p_o, which equals pressure reduced to sea level using another fictitious atmosphere: station temperature plus 0.65 °C/100 m going downward.
Of course, actual station pressure may be recovered from both, if needed.

For constructing surface pressure maps, I start out with the QNH, reported to the nearest hundredth of an inch. Adding 29 or 30 and converting to mb

$$1 \text{ inch} = 33.8642 \text{ mb}$$

we obtain what I call p_{QNH}.

As mentioned before, the technique is to do all computations, dynamical and hydrostatic, in terms of DP (see chapter 4.2). It turns out that approximately the DP at station height

$$DP \text{ (in meters)} = 8.35\ (p_{QNH} - 1013.25) \qquad (4.7)$$

When used without corrections, these airport DP-values don't permit smooth analyses. The following adjustments have been made:

- Minor individual systematic corrections for certain stations, determined by plotting contour maps for weak-gradient synoptic conditions, and by comparison with measured winds, the winds being assumed to be a fraction of the geostrophic wind, and to be pointing towards the lower pressure at angles between 30 and 70 ° (compare figs. 5.4 b and following).

- A DP observed at, say, Bradford (see fig. 2.1, elevation 655 m), may be allright for computing the average temperature between 850 and 950 mb (equ. 4.6, first line).
  When used in plotting a "surface" contour map on a reference level of ≈ 100 m MSL (Southeastern Pennsylvania) or, say, 1012 mb, in a synoptic situation with an upper trough (low DP), for example, the DP at Bradford will already be too low compared to representative "surface" values, being located almost halfway between the surface and 850 mb. It was decided, therefore, to obtain DP-values on reference p-surfaces by linear extrapolation, connecting 850 mb- and station values. This seems more appropriate than arbitrarily assuming either a standard atmosphere or a standard atmosphere shifted to station temperature in reducing station pressure to the reference level.

- There is a systematic difference between airport DP's and DP's computed from the soundings, the latter being lower by between 6 m (Pittsburgh) and more like 10 m (Washington). Such mismatches typically occur between two distinct observing systems; I could not research the cause. As I wish to operate with temperatures "calibrated" on the sounding temperatures, I applied the above negative, rather uniform correction term, which doesn't change horizontal gradients much.

- To get rid of random fluctuations of the reported altimeter setting, a (1 2 1)/4 time-smoothing is being applied throughout.

It should be remembered that pressure observations have an inherent inaccuracy of roughly half a mb or ≈ 5 m expressed in DP-units (equ. 4.7), and that synoptic surface pressure analyses are usually done at a 5 mb-interval. So, our 5 m-interval is really stretching the limit of what can be done, and only synoptic-scale features should be expected to show up in the observed and analyzed pressure fields.

5. Sequence of events

In the following I present a rundown of meteorological conditions from slightly before to a day after time Zero = March 28, 1979, 04 E.S.T. Fig. 5.1 is a map of the TMI area, covering a major part, but not all of the damaged tree evidence and other indications of acute radiation symptoms. The map may also serve to put the locations of the three closest wind measurements in topographical perspective:

TMI: On-site company-owned meteorological tower near the northern tip of Three Mile Island. Data source for the Defendants' official Gaussian segmented plume model calculations (Woodard, 1993). Strip charts available, with our own evaluation of 10-minute means and range of variability.

MDT: Present Harrisburg International Airport, located along the eastern shore of the Susquehanna River some 6 km northwest of TMI.

HAR: Harrisburg "Capital City Airport" along the western shore of the Susquehanna River, some 13 km slightly west of northwest of TMI.
For both MDT and HAR airports only one wind observation is available per hour, essentially an estimated 10 min.-average terminating near the hour.

For reasons of graphical convenience, all the presumed vertical temperature profiles at Harrisburg at three-hourly intervals are shown in one plot in fig. 5.2. All other maps and plots will be presented as time goes by. The techniques adopted for deriving these maps from the sparse upper-air data have been discussed in chapter 4. All times will be Eastern Standard Time, 27/18 being shorthand for March 27, 1979, 18 E.S.T.

Fig. 5.1 (next page):
Local terrain around TMI, with contours colored in 100 ft-intervals, and the two airport weather stations "Harrisburg" and "Middletown" marked. An improved version of fig. 7.1, p. 96, from part I.

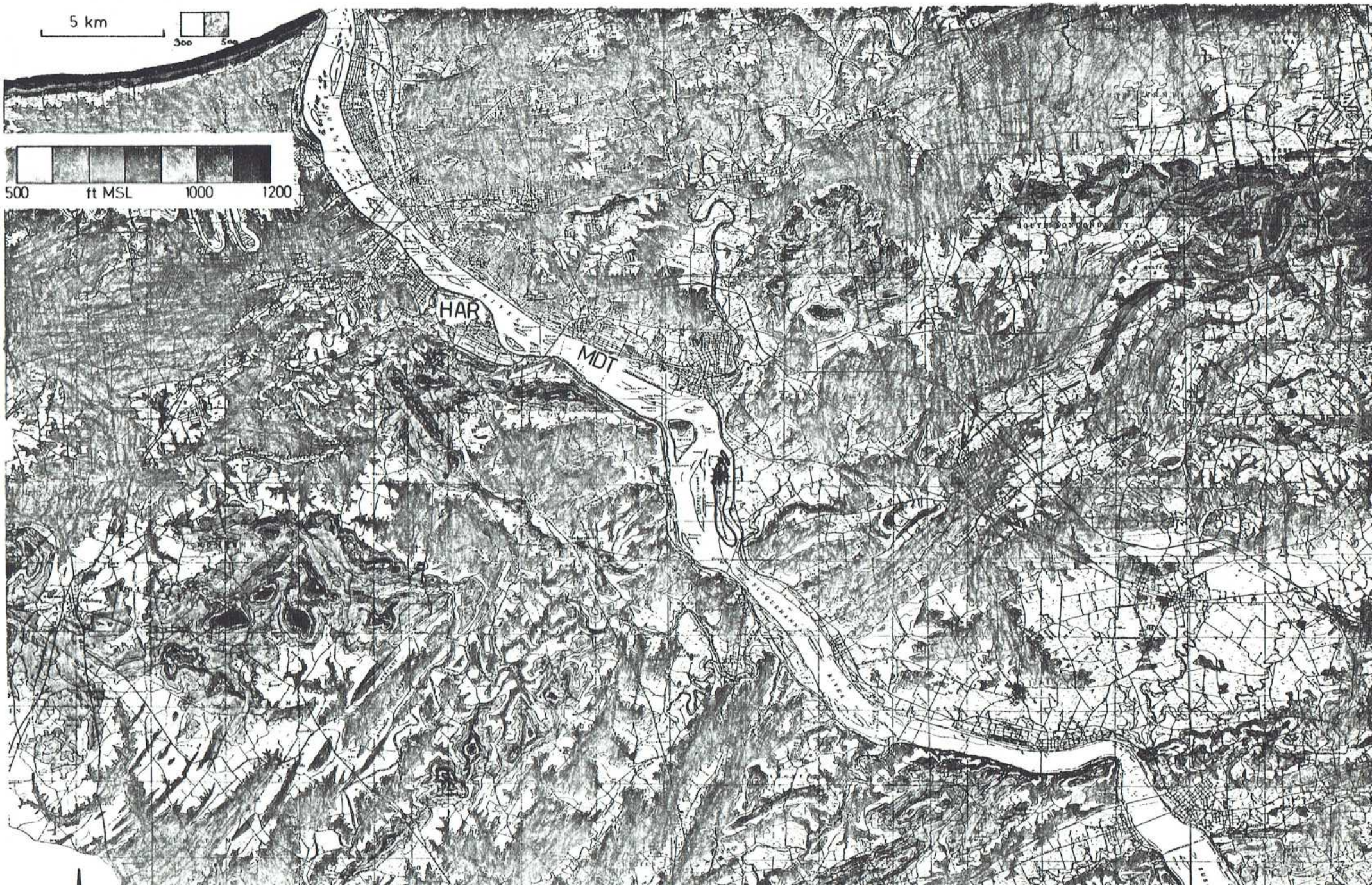
5 km
300
500
500
ft MSL
1000
1200
HAR
MDT

Fig. 5.2: *Approximate derived soundings for the Harrisburg area: Potential temperature profiles at 3-hourly intervals (see chapter 4).*

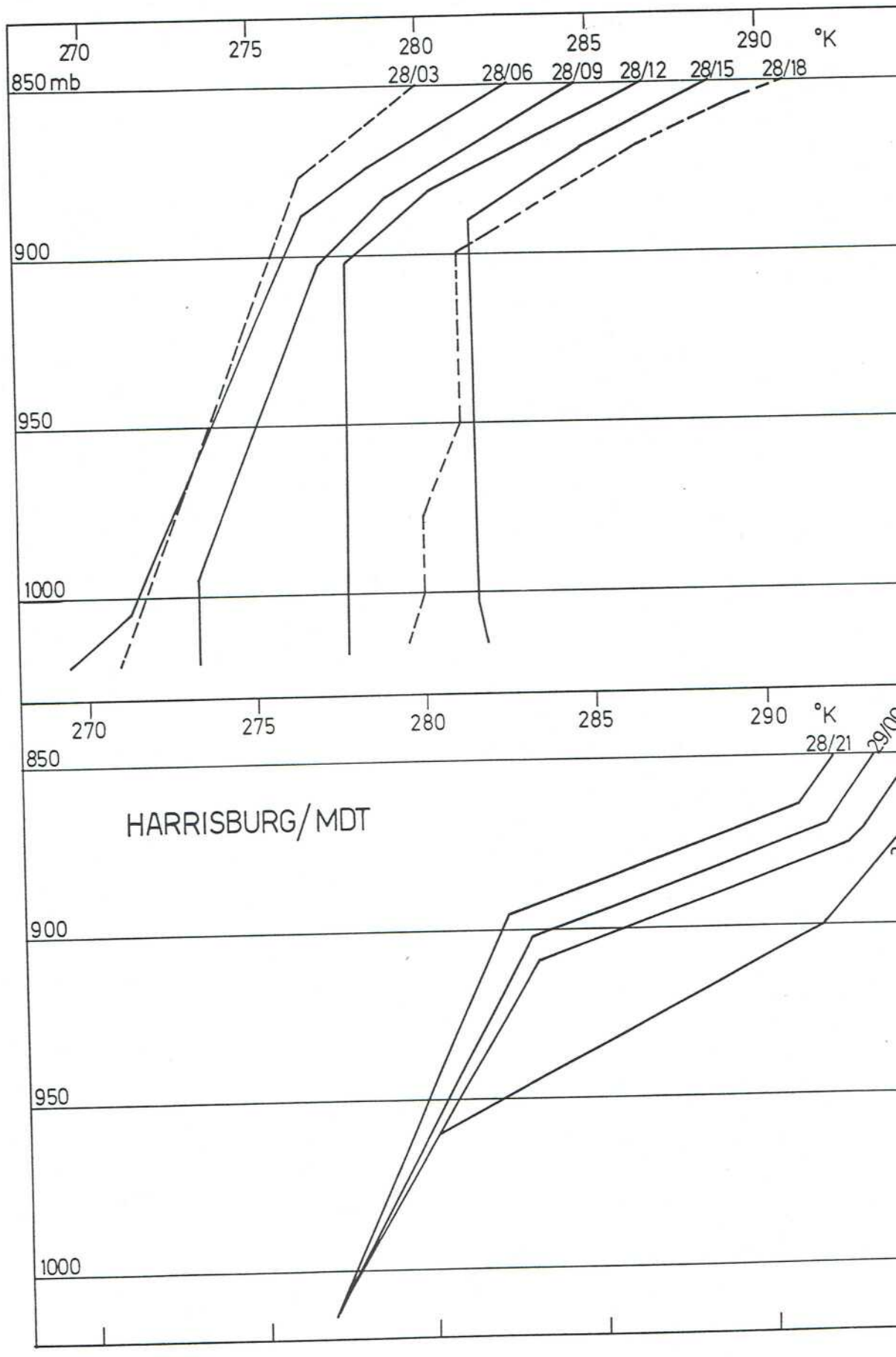

To establish continuity, upper-air contour maps (850 mb) are displayed first for 27/18 and 27/21 in fig. 5.3. A short-wave trough is seen to lie over Eastern Pennsylvania and propagate out of the area. The surface high is west of the Appalachians (no figure), and surface winds are westnorthwesterly all over the area. By midnight 28/00 (figs. 5.4), the surface pressure gradient has slackened considerably, and by 28/03 (figs. 5.5) the surface high is in the process of shifting over to the eastern slope of the Appalachian mountain range, giving the appearance of two mini-surges of cold air on either side. At 850 mb (fig. 5.5 a), an intermediary ridge of high pressure is seen to approach from the west, being centered right over Western Pennsylvania at 28/06 (fig.5.6 a). By that time, we are already two hours into the accident. The surface high is now located over Eastern Pennsylvania (fig. 5.6 b), but pressure gradients are very weak from the early morning hours into the late morning, and the structure of the general high pressure area over the Northeastern US is quite complex.

Surface winds west of the Appalachians begin to turn easterly by 2 or 3 a. m., responding to the reversed, if very weak, pressure gradient. They continue northwesterly to northerly, however, in the east, until 06 a.m., and even up to noon at some stations across Eastern Pennsylvania (see figs. 5.5 b and following). Across the east, there are many calms after 04 a. m. until 07 or 08 a. m.

There is a general turning of the winds towards northeasterly and easterly between 07 and 09 a. m., particularly south of the Pennsylvania border, and there is the Harrisburg/Middletown area, which stands out as an exception in that their airport winds turn easterly and even eastsoutheasterly as early as 06 a. m. (see the respective figures), with a notable disturbance at 10 a. m. (see fig. 5.7). In fact, TMI on-site winds turn from westnorthwesterly after midnight to northerly around 3 a. m. and to easterly as early as 5.30 a. m. (see the same figure).

Fig. 5.3:
Contours of the 850 mb-surface for the two indicated dates, expressed as DP in m (see chapter 4.2). Observed winds are plotted when available. Station in upper right corner is Albany, N. Y.
For techniques of derivation see chapter 4.

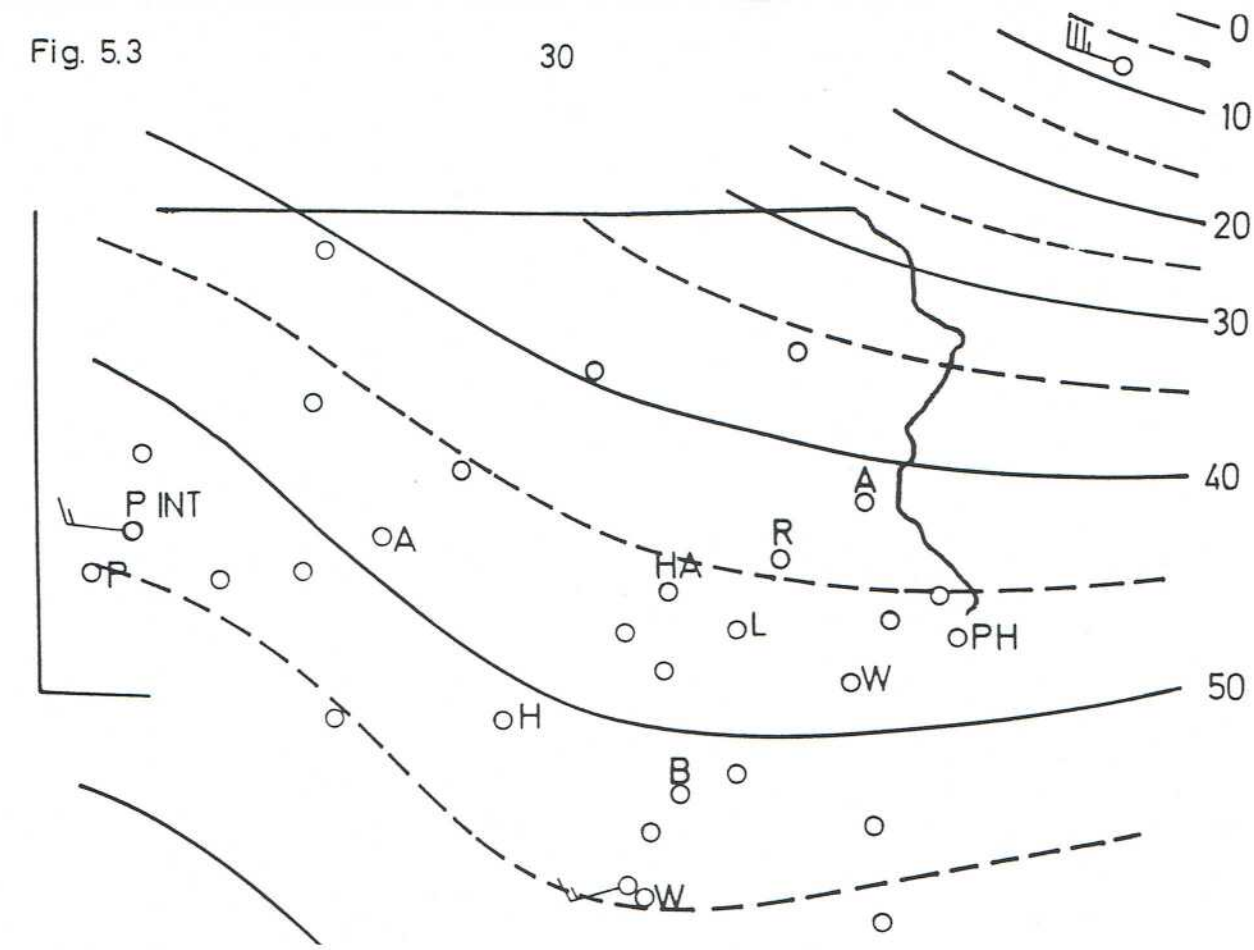
0
10
20
30
40
50
27.3
18 E
P INT
P
A
HA
R
L
PH
W
H
B
W
A

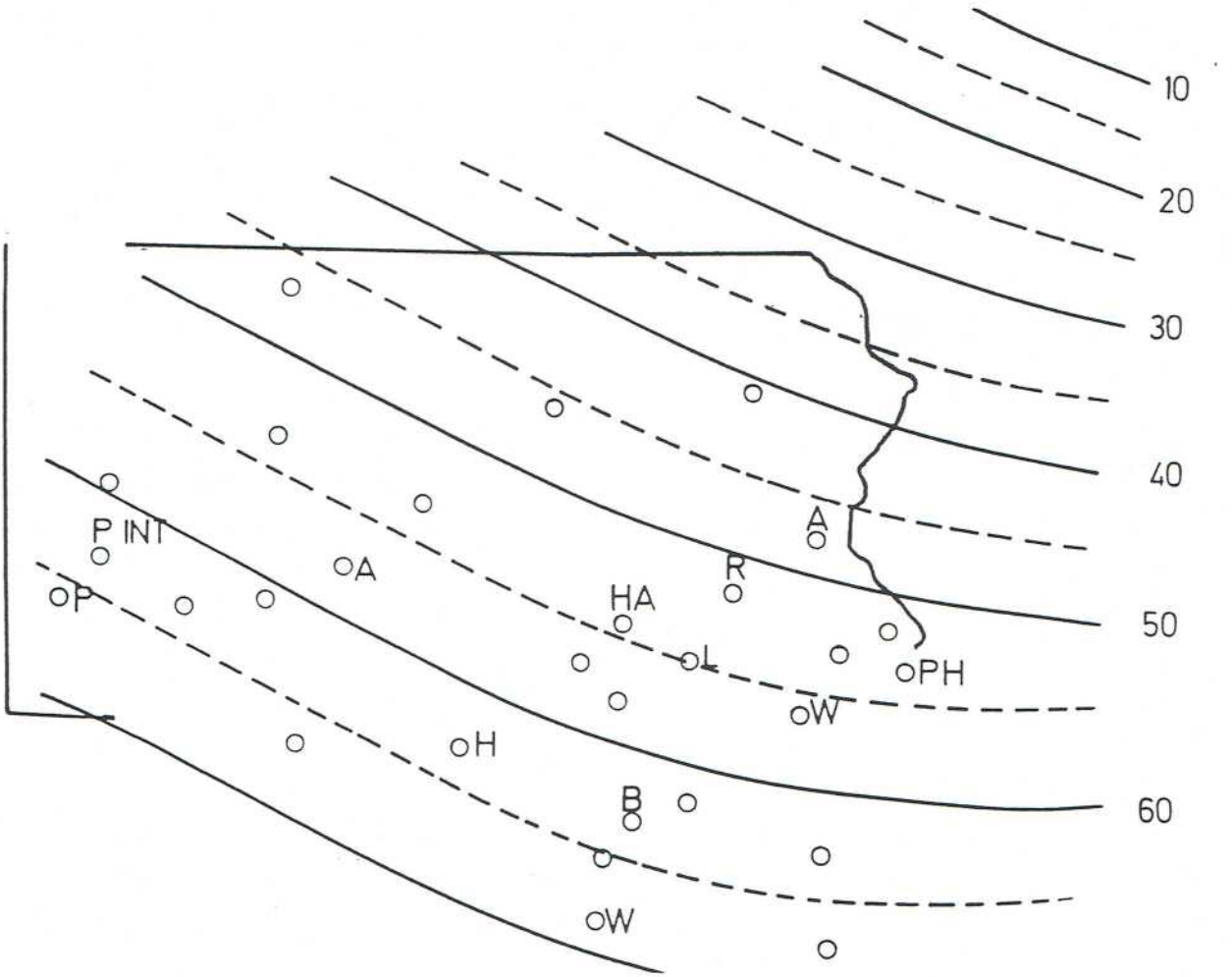
10
20
30
40
50
60
27.3
21 E
P INT
P
A
HA
R
L
PH
W
H
B
W
A

The general pattern of surface winds fits in fairly well with the contour lines of pressure or, equivalently, DP, as shown in the three-hourly sequence of maps. To interpret the three wind measurements available from the TMI area (fig. 5.7) in some detail is another matter. I will try, however, as these winds are the closest indication we have of transport directions and conditions in the vicinity of TMI.

At this point, I must refer to various other chapters: Slope winds in chapter 3, experience from the water tank experiments (chapter 7) and from the numerical model (chapter 6). The shallow-water-simulations tell us that the flow near hills, e. g. the TMI winds, in stable conditions can be deflected considerably from the general drift, as given by the water tank or the general surface flow. From fig. 5.2, the stratification must have been stable in the morning hours, but a very shallow mixed layer must have formed around 07 or 08 a. m., reaching a depth of ≈ 250 m by 09 a. m.

Returning to fig. 5.7, there is some synoptic sense in the early easterly wind directions around TMI, but to the best of my knowledge the slope wind circulations discussed in chapter 3 will also have played their part soon after 06 a. m., remaining very shallow at first, and also retarding the growth of the mixed layer over the lowlands via their compensating subsidence (see figs. 3.2 and 3.3).

It is quite possible, even likely from the general synoptic picture, that northerly flow components would have persisted for some time above that shallow surface-based layer, and that early TMI releases would have reached that level and been transported in various southerly directions first, before being carried westward.

Fig. 5.4 a (upper half) and b (lower half):
Simultaneous 850 mb contour map (upper half) and "surface" contour map (lower half) for indicated date. Both are expressed as DP (m) (see chapter 4.2).
"Surface" is meant to indicate that all DP's have been extrapolated or interpolated to a level ≈ 100 m MSL (Eastern Pennsylvania) corresponding to ≈ 1012 mb (see chapter 4.3). Erroneously, the German T (Tief) has been plotted instead of L (Low). Observed airport winds are entered in the usual SYNOP key (1 full barb = 10 knots), as well as total cloudiness. For station initials see fig. 2.1.

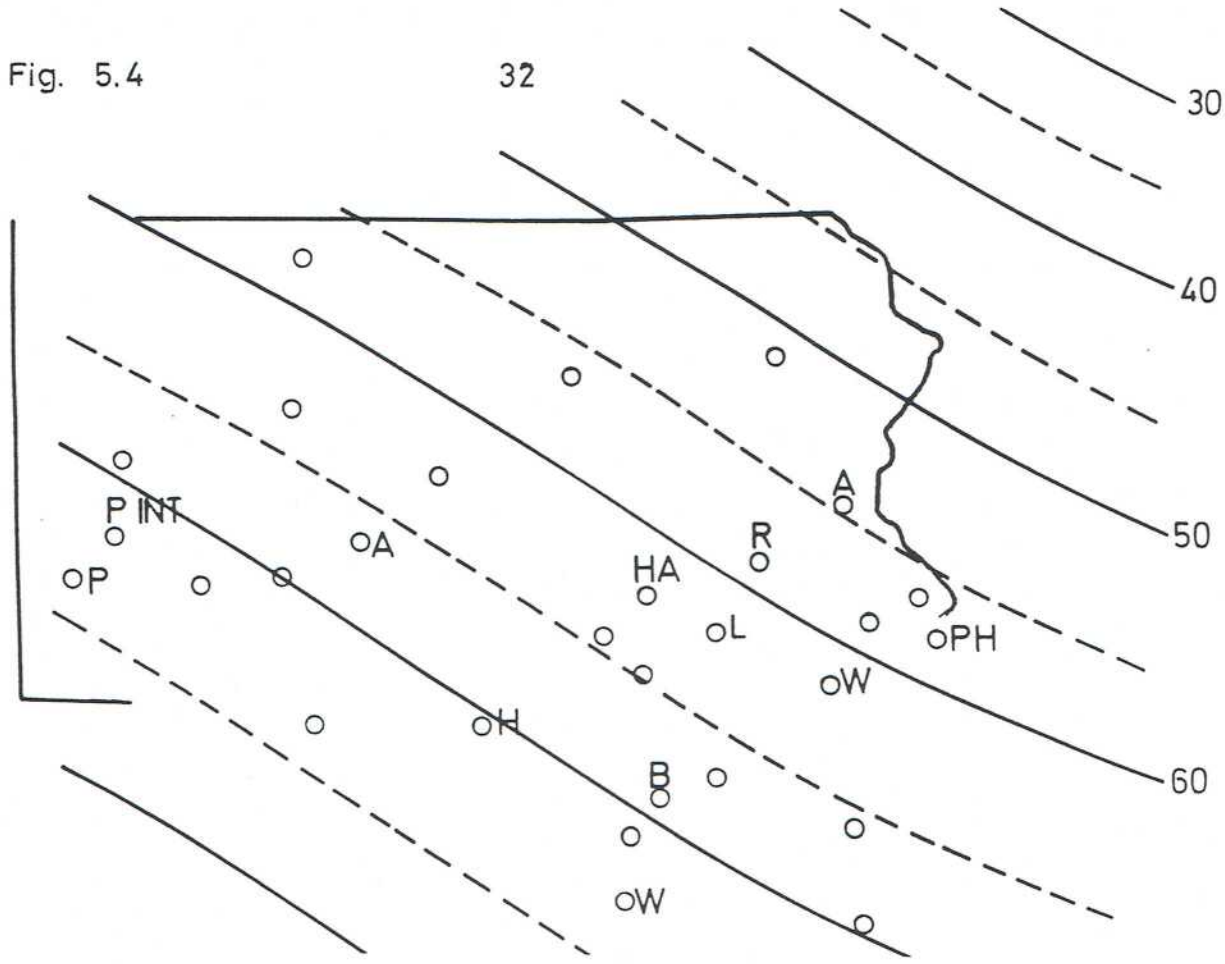
30
40
50
60
P INT
P
A
HA
R
L
W
H
B
PH

28.3.79 00EST

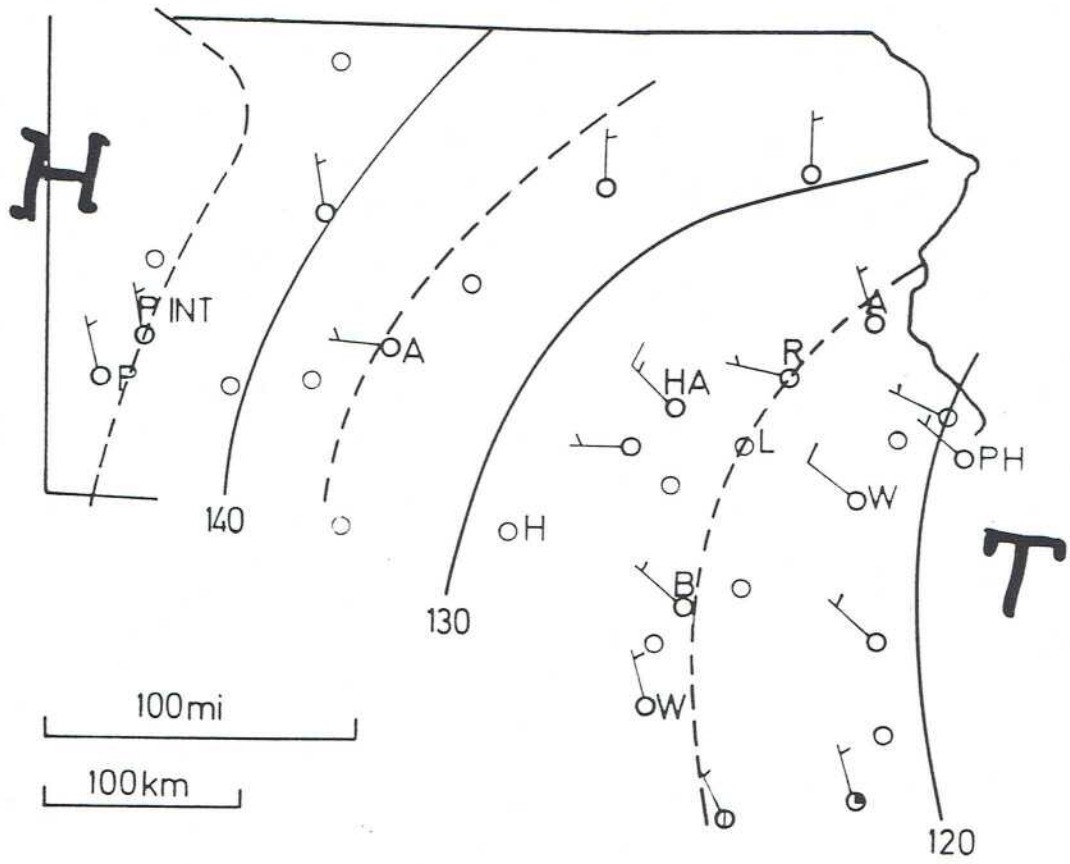
H
P INT
P
A
HA
R
L
W
PH
H
B
140
130
120
100mi
100km

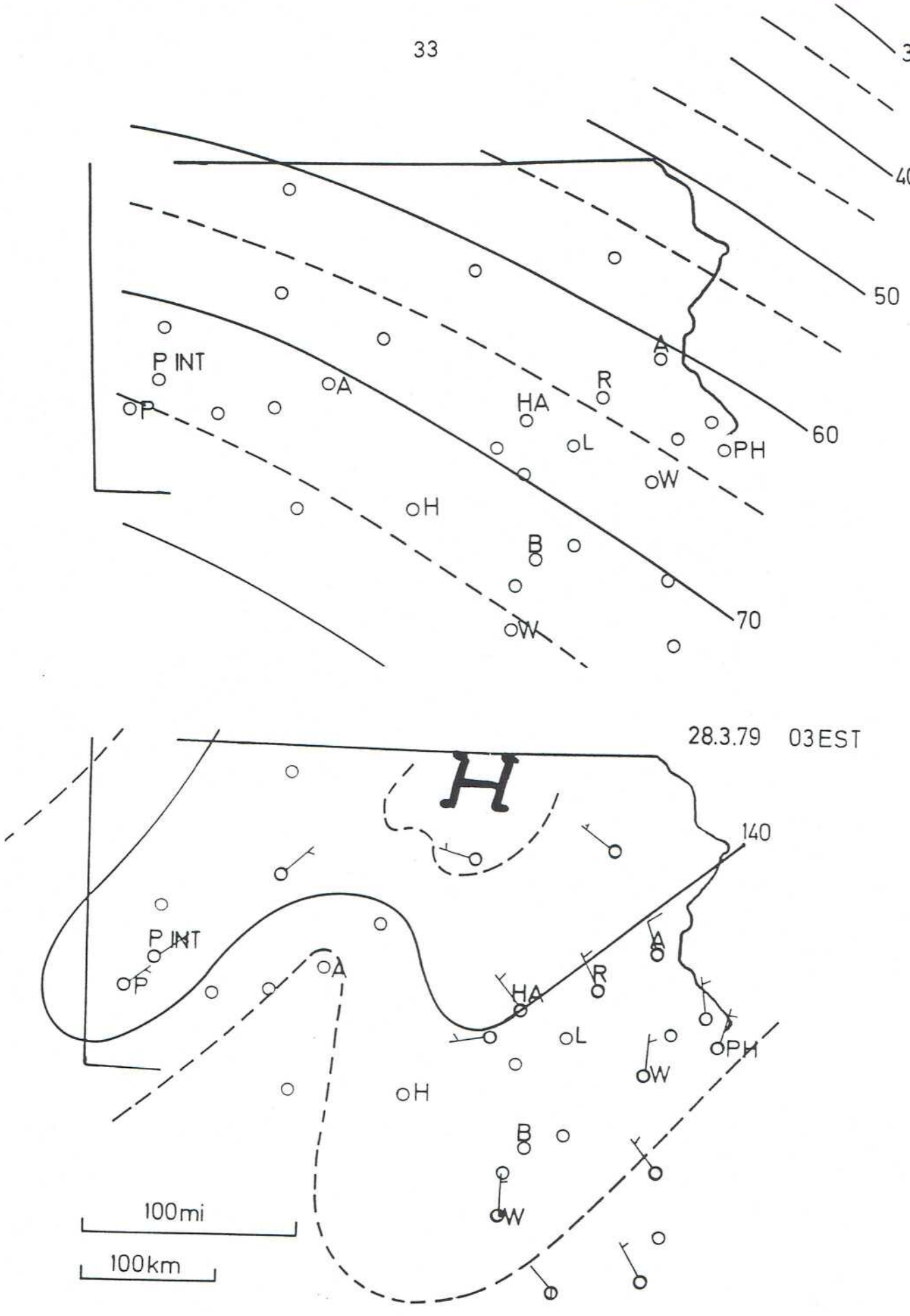

Fig. 5.5: *850 mb and surface maps for indicated date. See fig. 5.4*

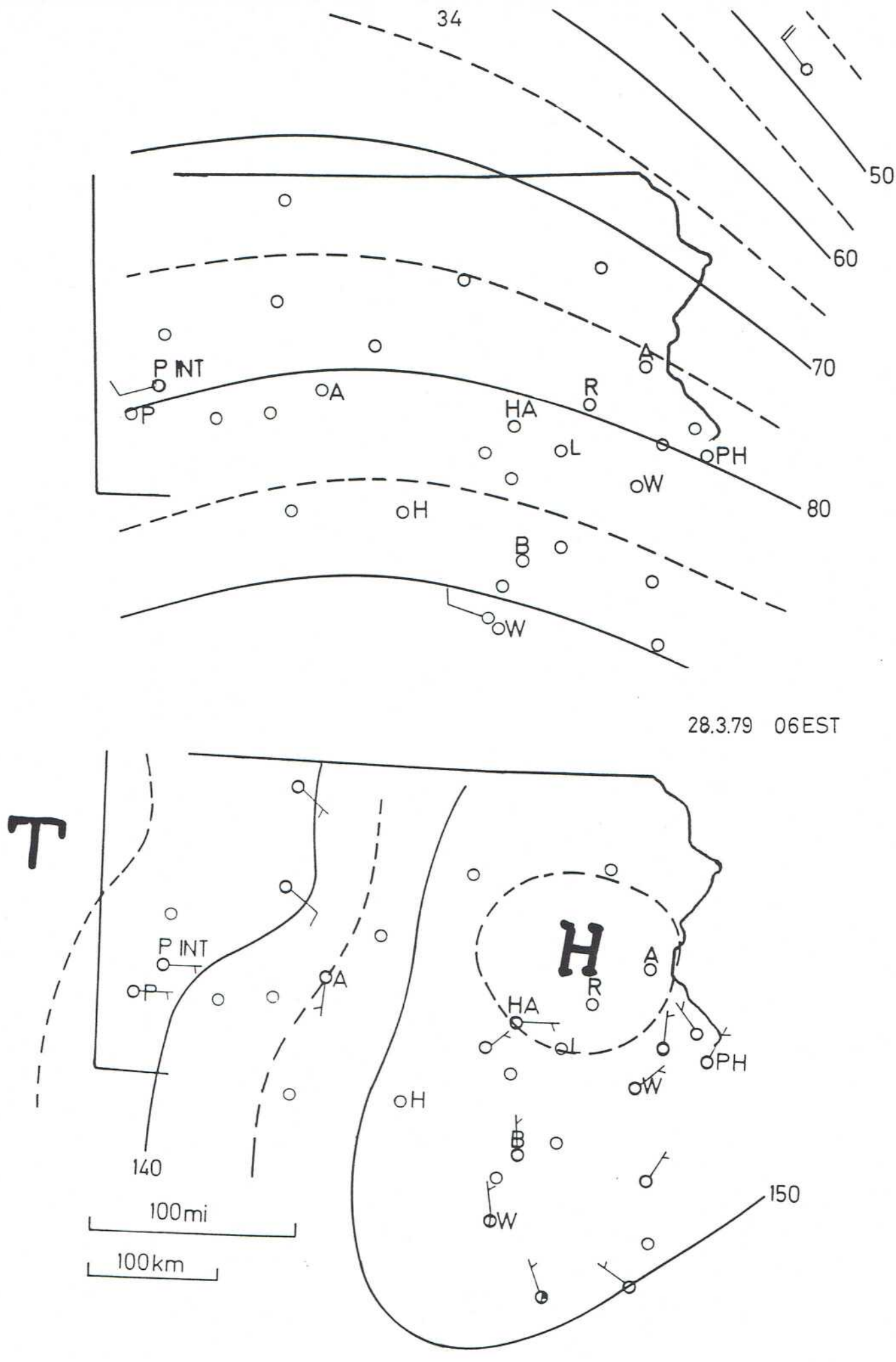

Fig. 5.6: *850 mb and surface maps for indicated date. See fig. 5.4*

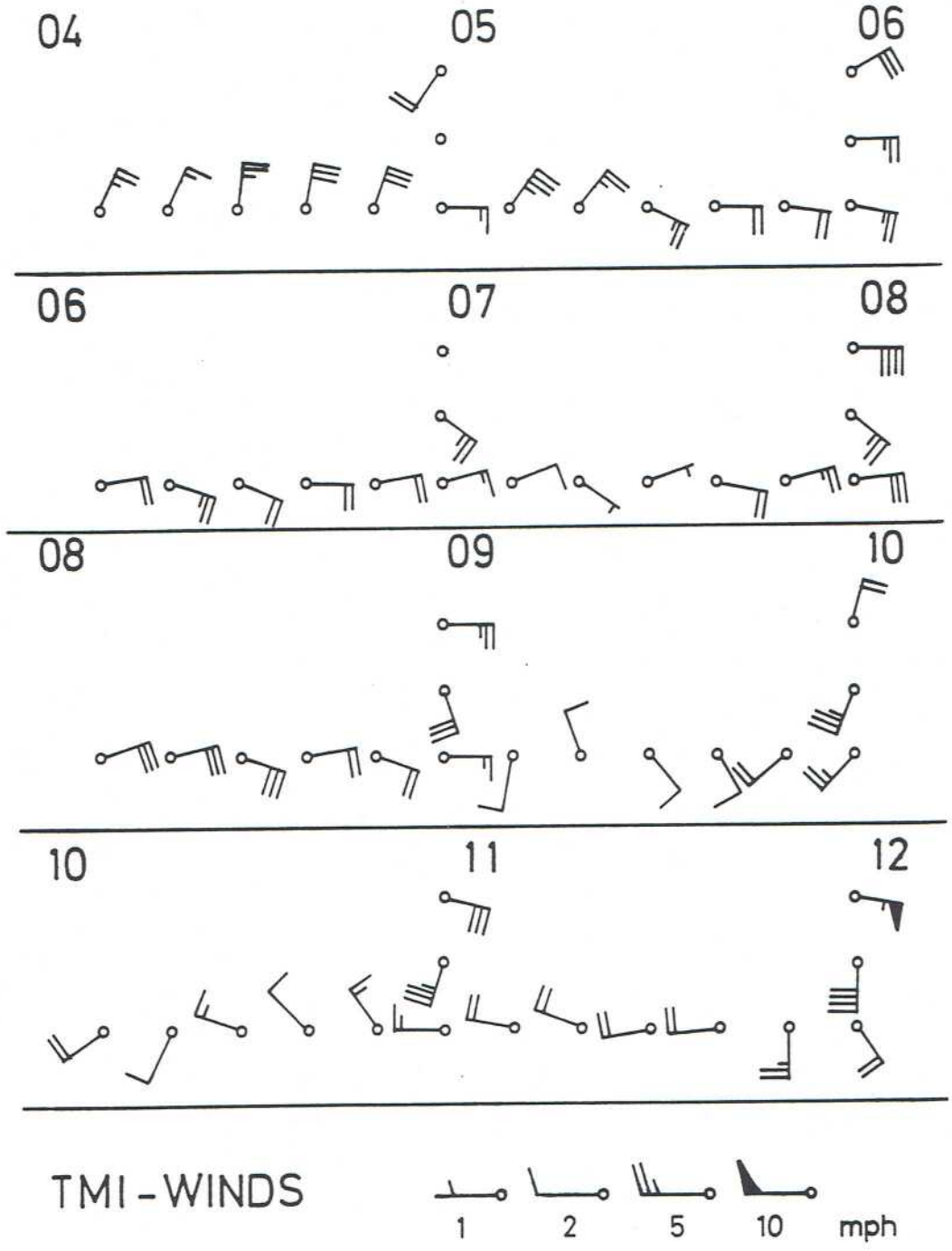

Fig. 5.7:
TMI Met Tower Winds for March 28, 1979, 04 - 12 E.S.T.
10-minute averages, mph see scale.
On top of each line, the once-an hour airport winds observed at HAR (above) and MDT (below) have been entered. Strictly speaking, these are in knots, but the difference is not worth bothering, as

1 kn = 1.15 mph = 0.515 m/s

Remnants of down-valley flows, sandwiched above the shallow upslope currents, may have joined the northerly flow (see chapter 3). This was still a situation of low-level cold-air advection, so turning of the winds from near easterly at the surface via northeasterly and northerly to westnorthwesterly at 850 mb (fig. 5.6 a) would make synoptic sense. Along these same lines, the Washington sounding between 06 and 07 a.m. (fig. 2.2 c), far away from slope influence, still has light northerly to northwesterly winds all the way up to 850 mb ≈ 1500 m MSL.

Considering all this evidence, the conclusion is inescapable that the TMI tower winds at 100 ft a. g. are not necessarily representative of the real transport directions at effective release height.

The SSW wind reported at HAR at 5 a. m. (fig. 5.7) adds to the picture of highly confusing wind currents , and the plot of 10-minute wind averages evaluated from the TMI tower data highlights the variability and nonstationary character of these fairly light winds, which fact will be important for the interpretation of stationary simulation experiments (chapters 6 and 7). Note that the 10-minute winds themselves are again averages over considerable fluctuations of direction and speed, not shown any more in fig. 5.7.

Any radioactive plumes and puffs drifting about with very little dispersion in these highly stable and changeable wind fields, and being "sucked" into slope wind currents here and there along the wooded hills, would be subject to "fumigation" = downmixing to the hill slopes, as soon as the mixed layer reached the level of releases around ≈ 8 a. m. (see also part I, chapter 7).

The maps for 28/09 (figs 5.8) show the upper ridge right over Eastern Pennsylvania. At the surface, winds and contour lines suggest a last surge of cooler air from the northeast across Eastern Pennsylvania and further south. Because of the strong insolation, this surge doesn't leave much of a signature in the surface temperature field, but it does in the surface pressure field, and, as a consequence, in the average temperature $\overline{\Theta}$ between 850 mb and the surface (see chapter 4). Consider the following little table, in which the two stations may be taken to be representative for the Western Plateau and the Eastern foreland, respectively:

Hour-to-hour local change of the vertical mean (potential or actual) temperature between 850 mb and the surface = $\partial\overline{\Theta}/\partial t$ in ° C per hour.

March 28/1979	06-07	07-08	08-09	09-10	10-11	11-12	a. m.
Pittsburgh	1.0	1.2	2.3	1.0	1.9	2.6	
Harrisburg	0.2	0.5	0.9	−0.2	0.5	1.7	

Note that the phase of gradual warming to be expected between 06 and 09 a. m. is being disrupted by an actual slight cooling at Harrisburg between 09 and 10 a. m., and, in fact, at all stations across Eastern Pennsylvania, Maryland and Delaware! This very significant temperature depression continues between 10 and 11 a. m., fading away thereafter towards noon. It could not be an artifact of the interpolated 850 mb contour maps (see chapter 4.1), as these 3-hourly maps are very smooth, and have been linearly interpolated down to 1 hr-intervals.

The temperature changes at Pittsburgh are less straightforward to interpret. There is no actual cooling, but there is a depressed temperature rise between 09 and 10 a. m. and a bit further, which could be the result of forced convergence and upward motion.

Pursuing the trace of this last surge of cold-air advection in the winds and contour lines, an intermediate surface map at 11 a. m. (fig. 5.9) has the cool surface high displaced southward, compared to 09 a. m., with most of the winds rather confusing in this weak-gradient region, but at least the southerly to southeasterly direction at HAR/MDT and the westerly components at Lancaster and Reading marginally compatible with the synoptic mesoscale high.

The detailed winds in the TMI area (fig. 5.7) pose more questions than we can answer. To begin with, there is the odd northnortheasterly wind at HAR at 10 a. m. Then, there is a two-hour period between 09.40 and 11.40 a. m. when TMI-tower has southwesterly to northwesterly winds, before finally the southerly to southeasterly flow pattern characteristic for the rest of the day becomes established by noon. These odd winds certainly cannot be explained by thermal forcing. A plausible conceptual model is to imagine the air parcels following the cool-air surge from the NE turning around towards the right in the manner of an "inertial circle", as they drift into a region of vanishing pressure gradient, such that the deflecting action of the earth's rotation can become dominant.

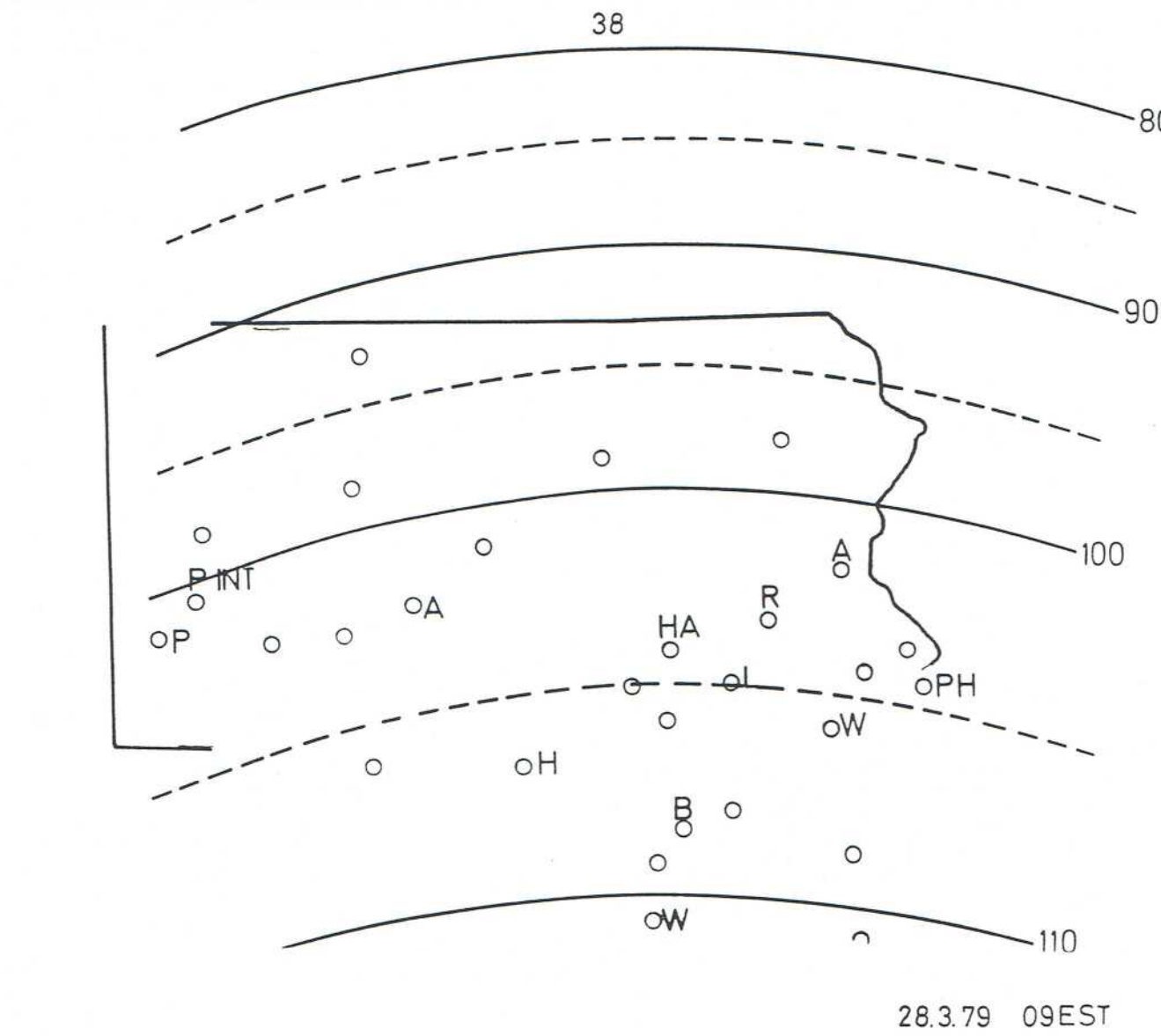

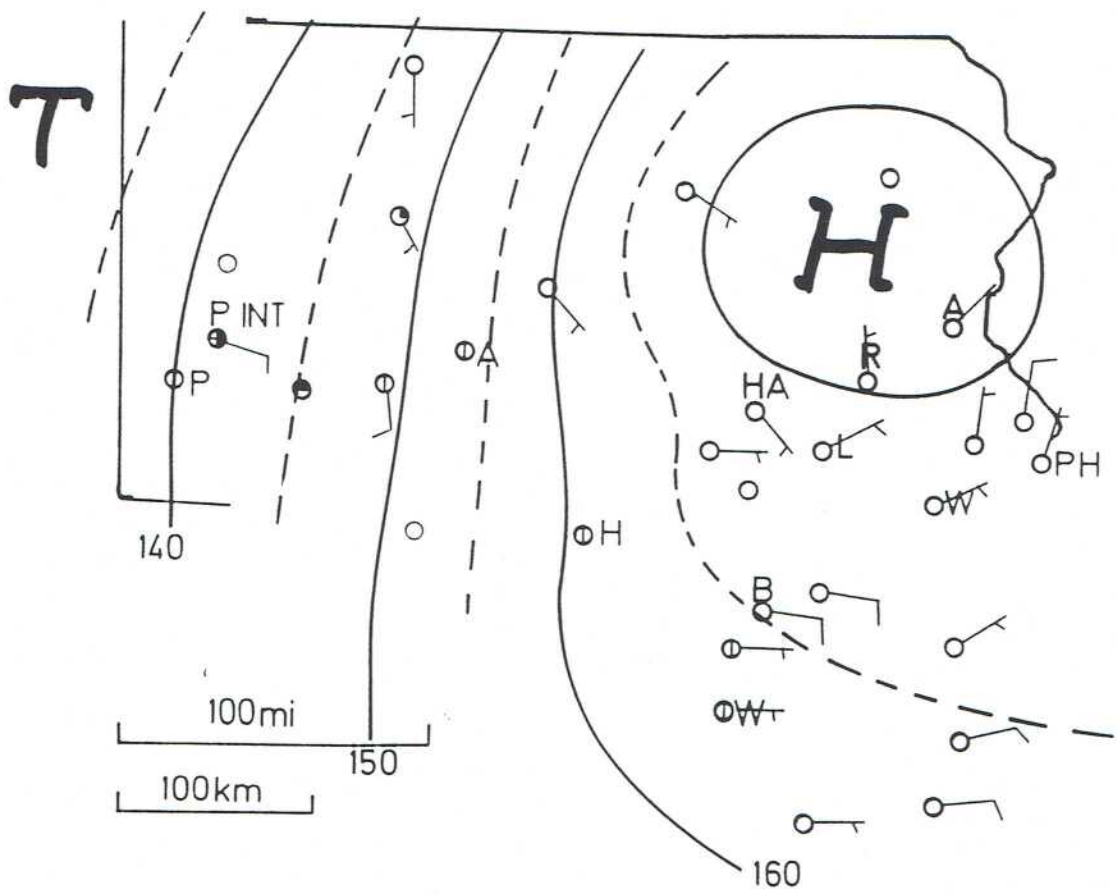

Fig. 5.8: *850 mb and surface maps for indicated date. See fig. 5.4*

Consequently, winds along such a trajectory would turn easterly (see fig. 5.8 b), then southerly and westerly, with some possible reflecting influence of the Appalachians. These winds could point against any local residual pressure gradient force, until the air parcel's kinetic energy had been exhausted.

Westerly winds are not evident either at Harrisburg or at Middletown. This may be due to local channeling of the flow or to resumed prevalence of upslope or upvalley circulations near the valley floor, but certainly these late morning hours stand out as extreme examples of diverging winds within a distance of less than 10 miles, and all at fairly well-exposed observation sites!

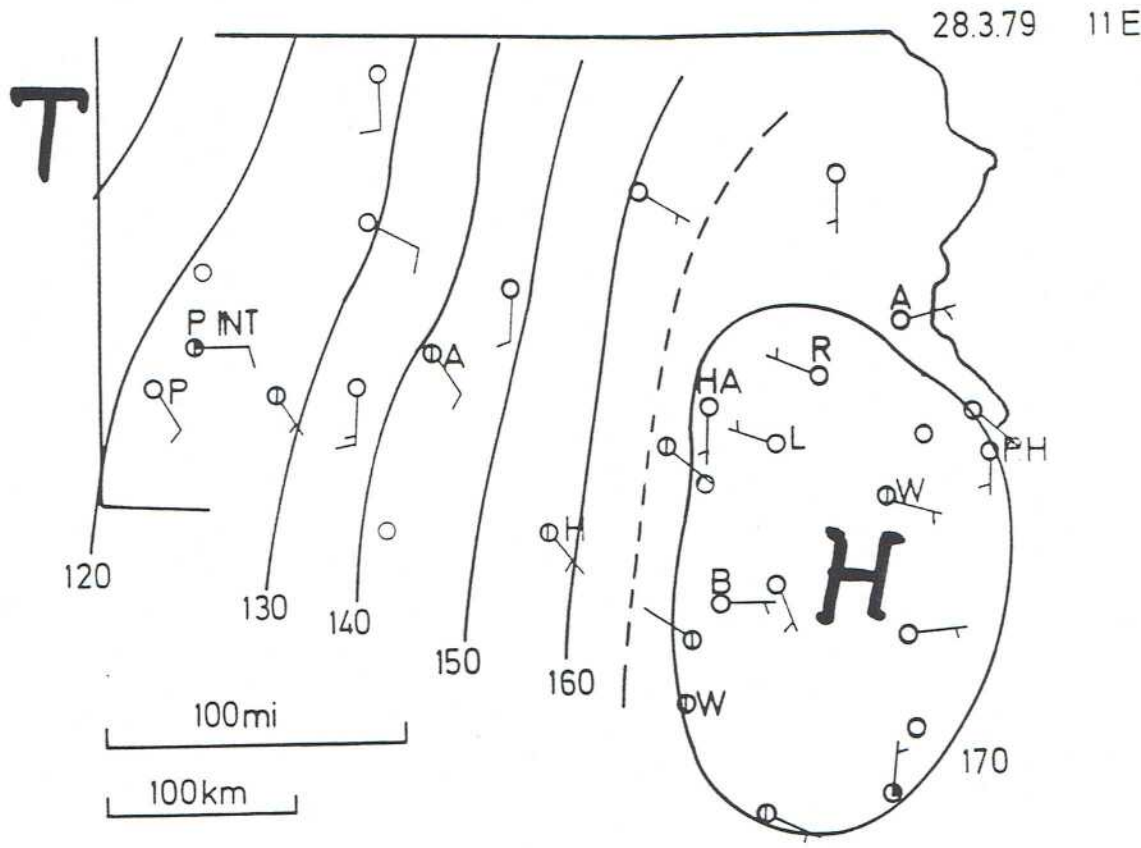

Fig. 5.9: *Surface map for indicated date. See fig. 5.4*

With a final westnorthwesterly wind reported from Lancaster at 12 E.S.T. (fig. 5.10 b), this late disturbed episode makes way for the typical prefrontal flow pattern for the rest of the day (figs. 5.10 to 5.14). At upper levels a short-wave trough approaches from the west, and winds at 850 mb on its eastern flank strengthen and veer from westerly to southwesterly.

The accompanying warm-air advection has been amply documented. At the surface, the pressure gradient across the Appalachians strengthens, with the observed winds across Eastern Pennsylvania and southern forelands picking up to reach 10 or 15 knots in places, and blowing cyclonically around the low pressure center out west, with a typical frictional deviation of ≈ 40 ° or so pointing towards the lower pressure (DP). Hourly winds at TMI, HAR and MDT have been plotted in part I, fig. 2.3. The three winds don't agree perfectly by any means, but they do blow generally from the south or southsoutheast. As a mixing layer ≈ 1 km deep has been established around noontime and early afternoon, we expect that there would only be a slow turning of the wind with height, from SSE near the surface via S to SW or WSW at 850 mb. In this case, the frictional deviation expected is in line with the sense of wind turning characteristic of warm-air advection.

Later in the afternoon, after 4 p. m. or so, I expect the ground to begin to get cooled and to accumulate cooler air, very shallow at first, in sheltered low-lying places. Fig. 5.2, of course, can show this process of beginning stabilization from below only very schematically. The reader who noticed the clouds moving in towards the afternoon may wonder about the cooling, but these clouds are high- and middle-level clouds at most, and they clear away completely once more from after 7 p. m. to shortly before midnight (see fig. 5.13 and part I, fig. 2.3). The temperature trace (fig. 2.3), too, confirms the cooling until 9 p. m or so.

The difficult and little-researched evening transition phase from mixed layer to stable boundary layer has been repeatedly quoted (see also chapter 8). Referring to my part I, chapter 6 and also chapter 3, some symptoms of beginning stagnation at the lowest levels are discussed there, evident both in the observed winds turning eastsoutheasterly (figs. 5.15 b, 5.16 b and part I, fig. 2.3) and in the regional model simulations. Stagnation would be too shallow at first to leave a signal in the pressure (contour) field. Not before the early morning hours of March 29 do we see signs of a slackening pressure gradient across Eastern Pennsylvania (figs 5.15 b, 5.16 b), whereas it tightens across Western Pennsylvania (see also the last column of winds for 29/07 on the Pittsburgh sounding fig. 2.2 a).

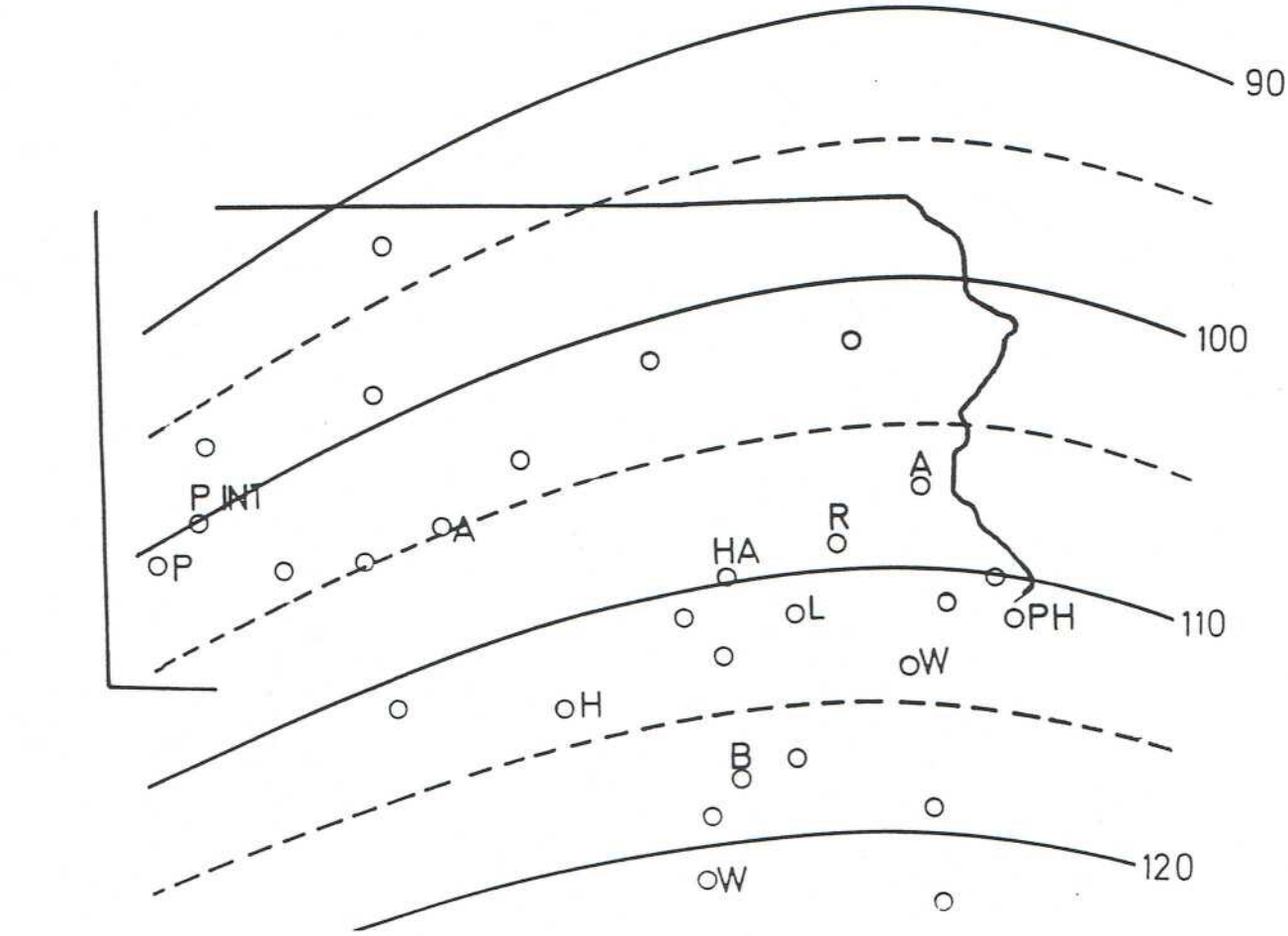

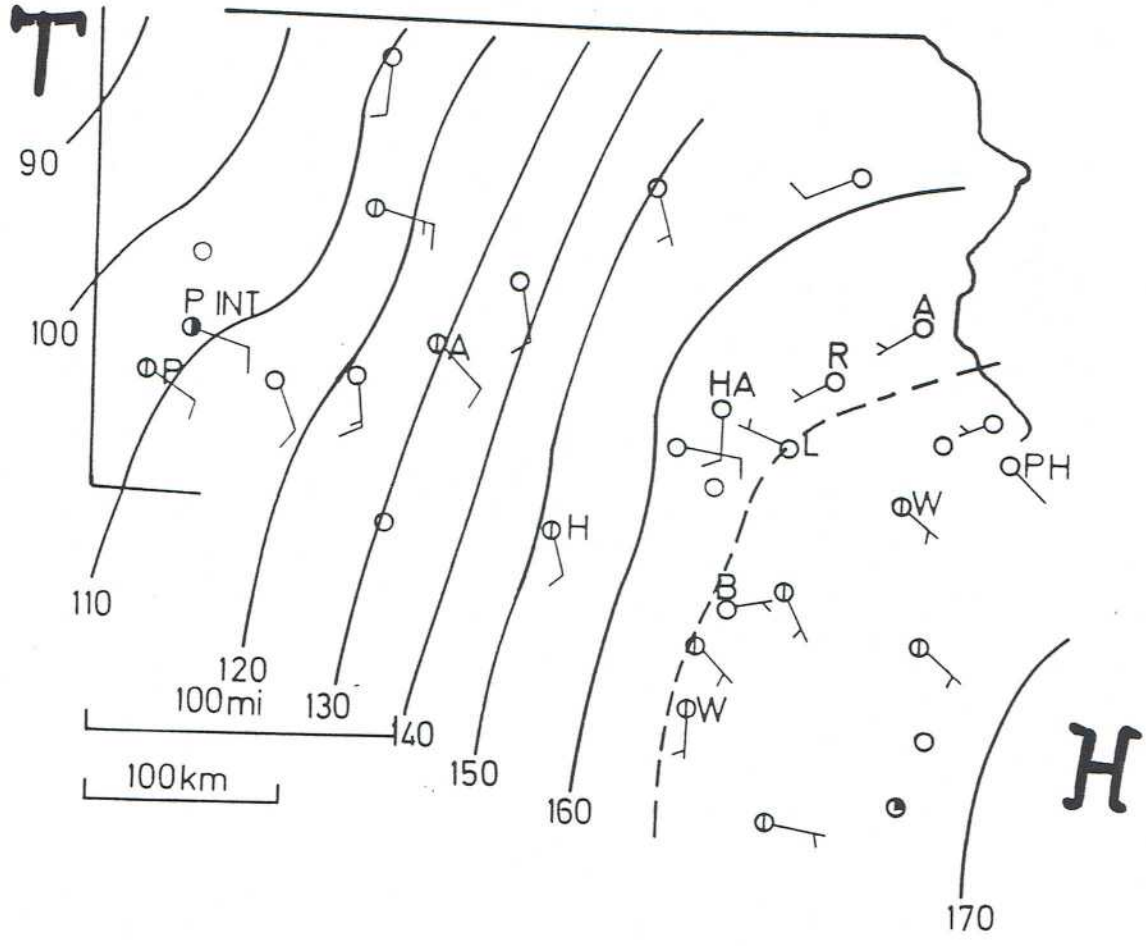

Fig. 5.10: *850 mb and surface maps for indicated date. See fig. 5.4*

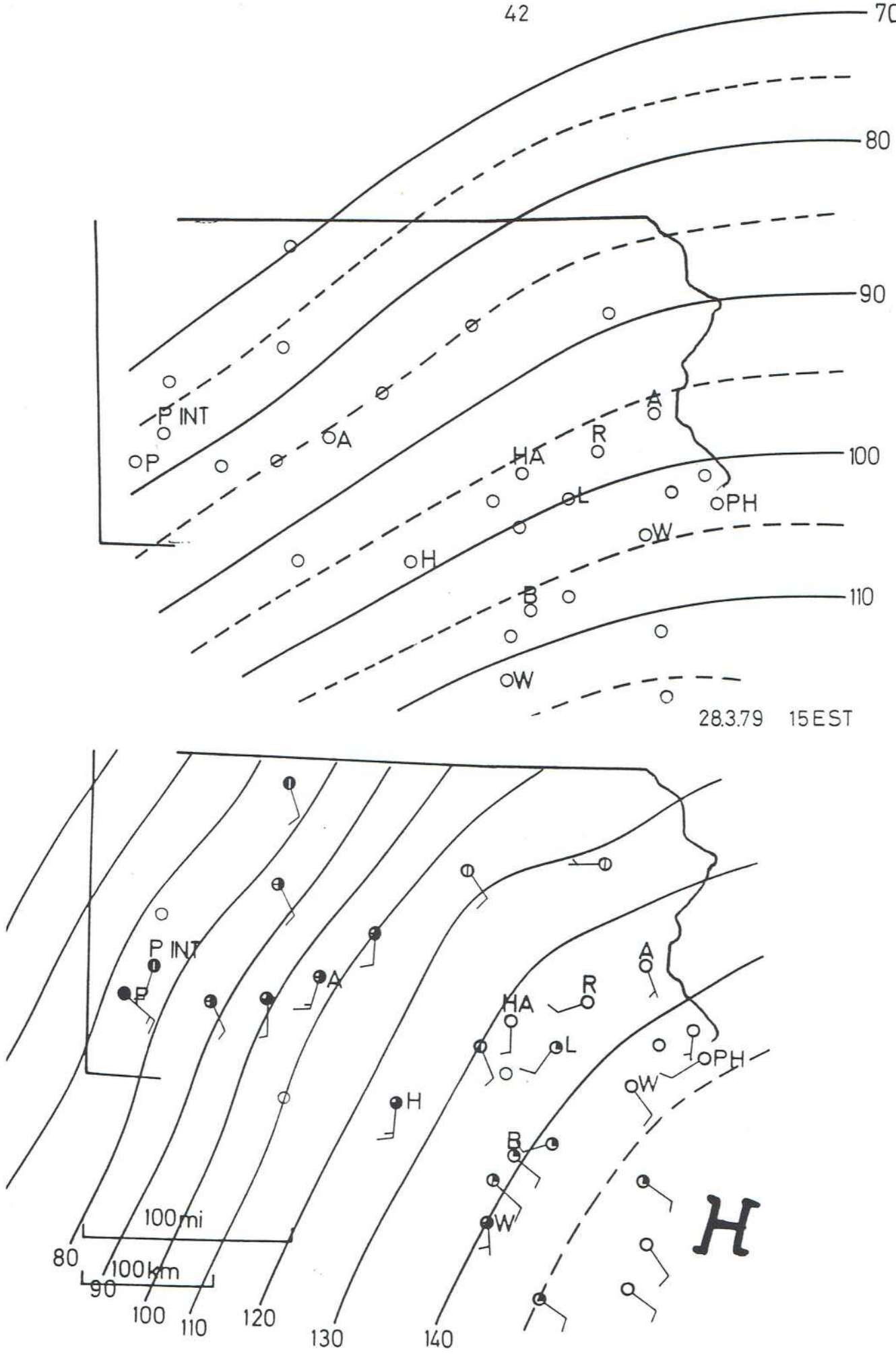

Fig. 5.11: *850 mb and surface maps for indicated date. See fig. 5.4*

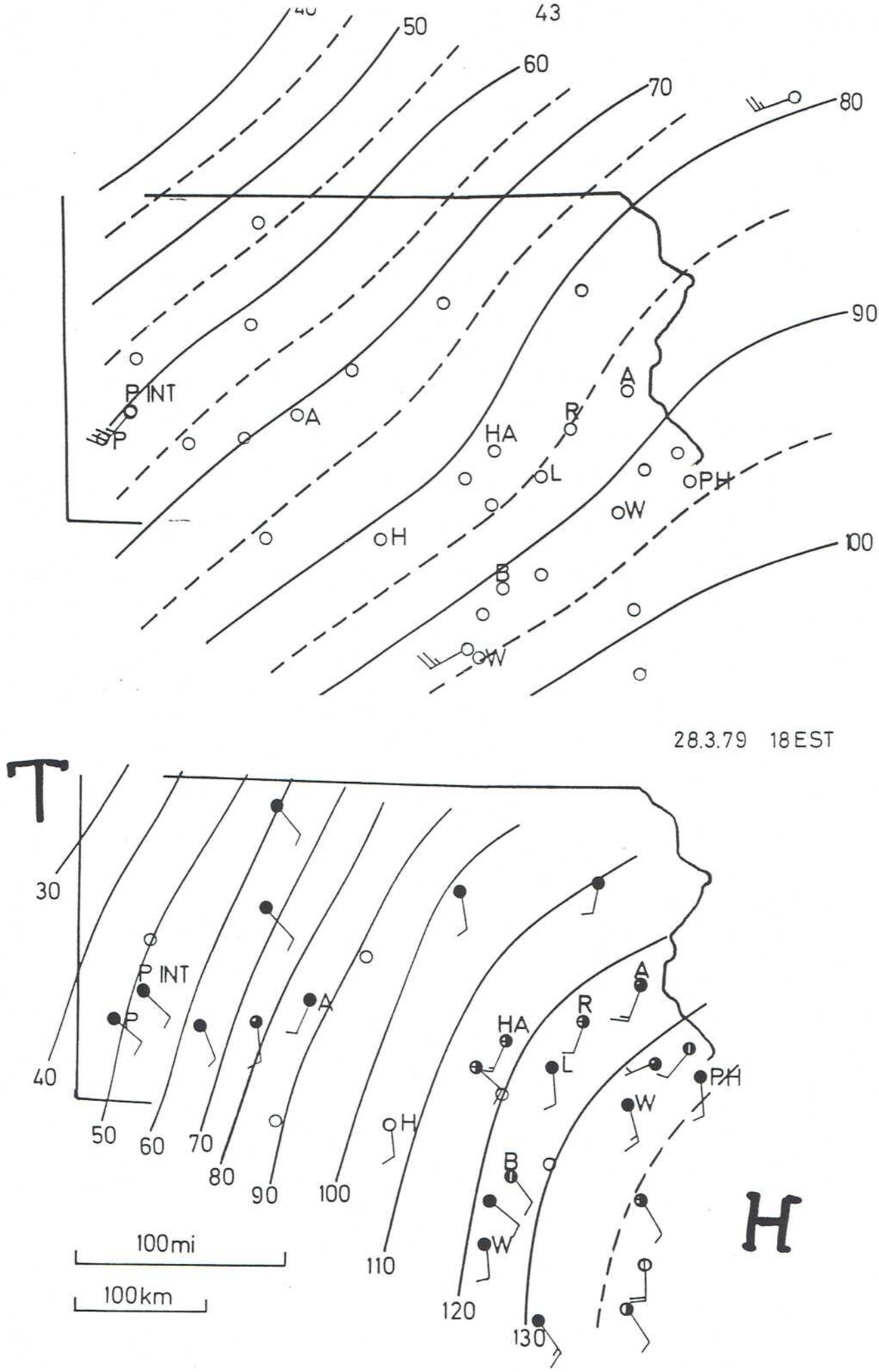

Fig. 5.12: *850 mb and surface maps for indicated date. See fig. 5.4*

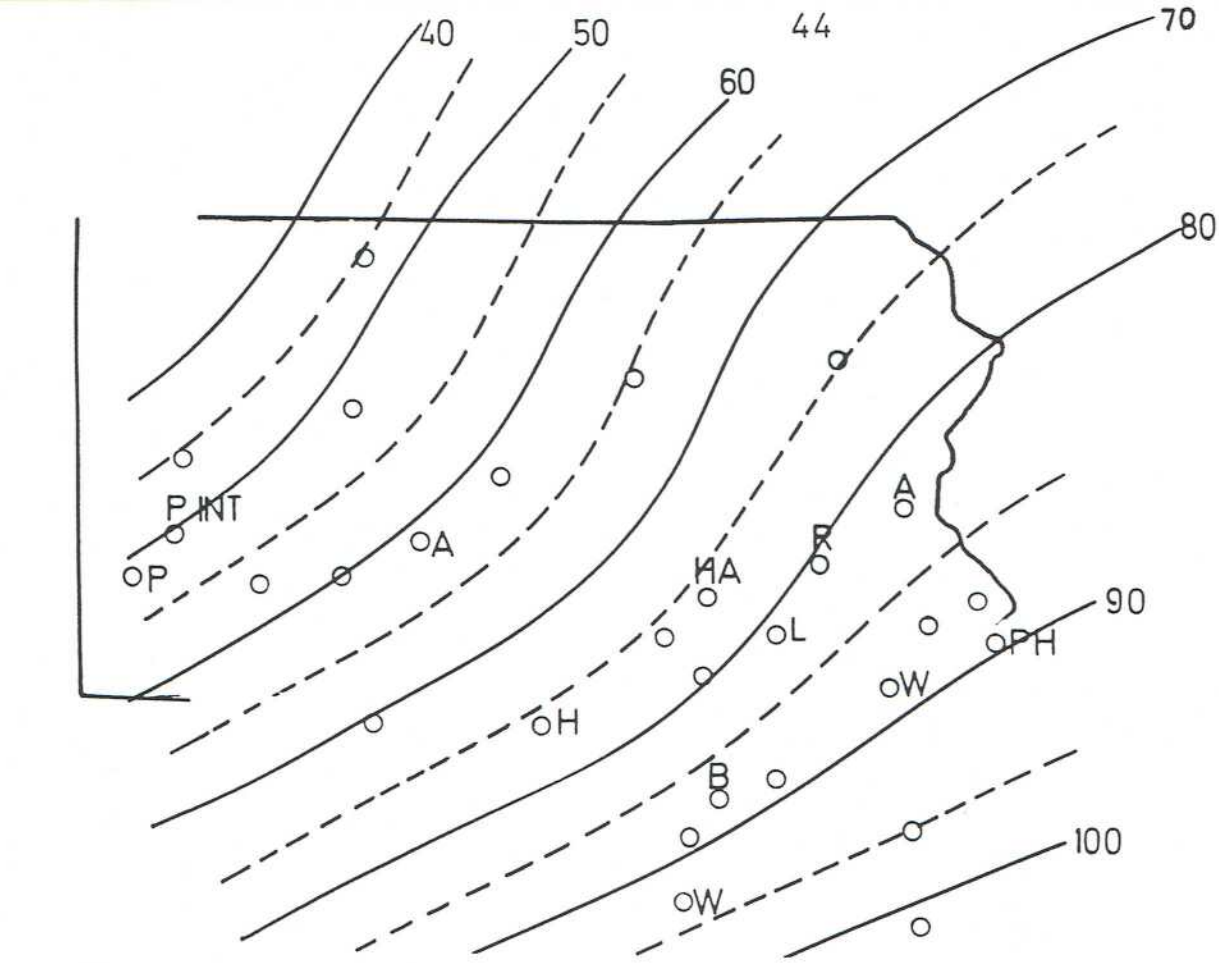

28.3.79 21EST

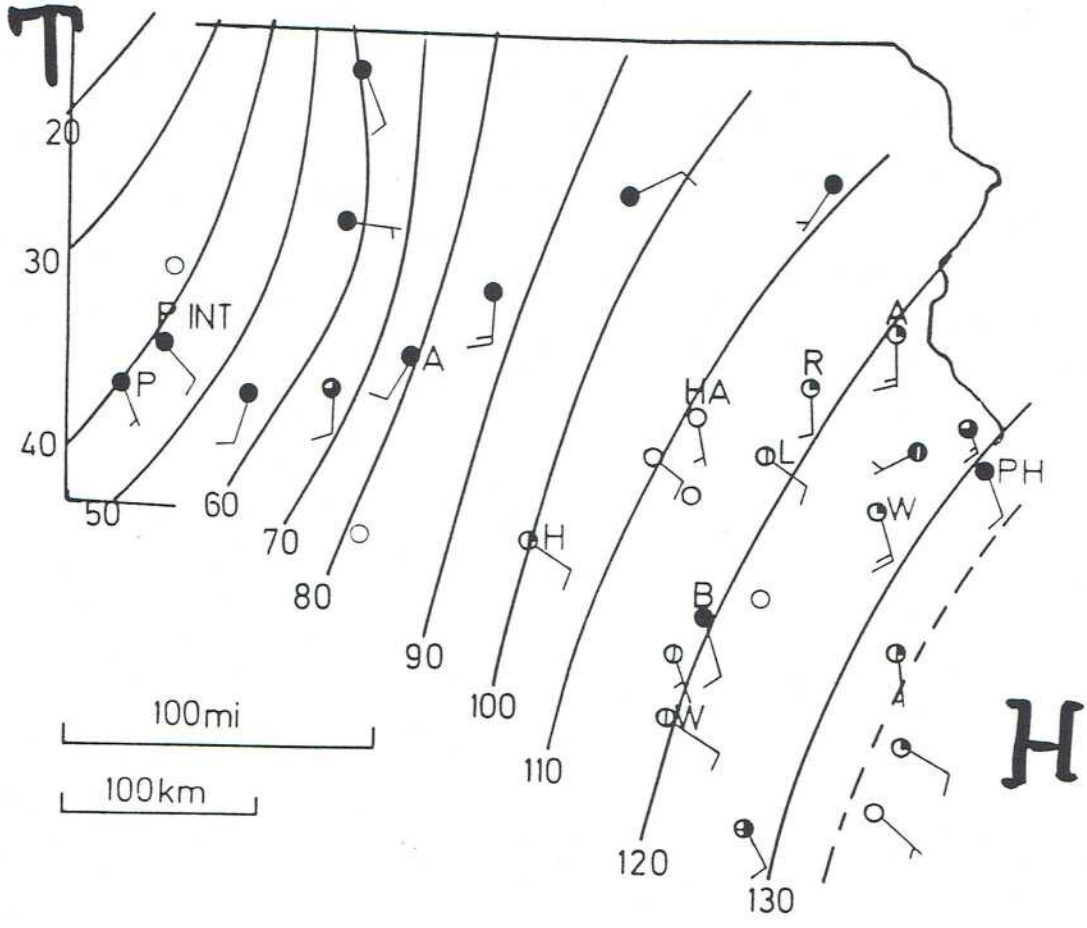

Fig. 5.13: *850 mb and surface maps for indicated date. See fig. 5.4*

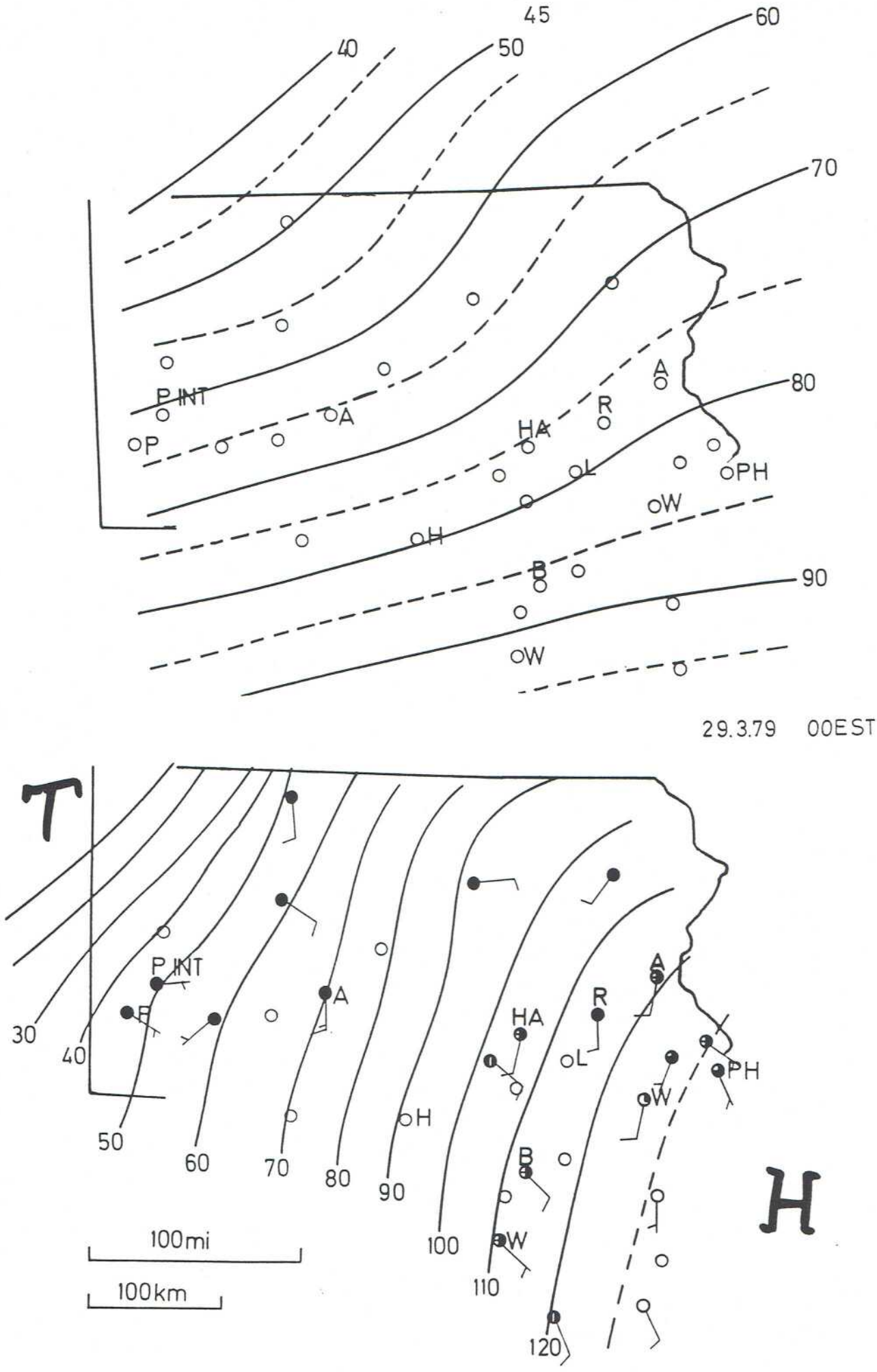

Fig. 5.14: *850 mb and surface maps for indicated date. See fig. 5.4*

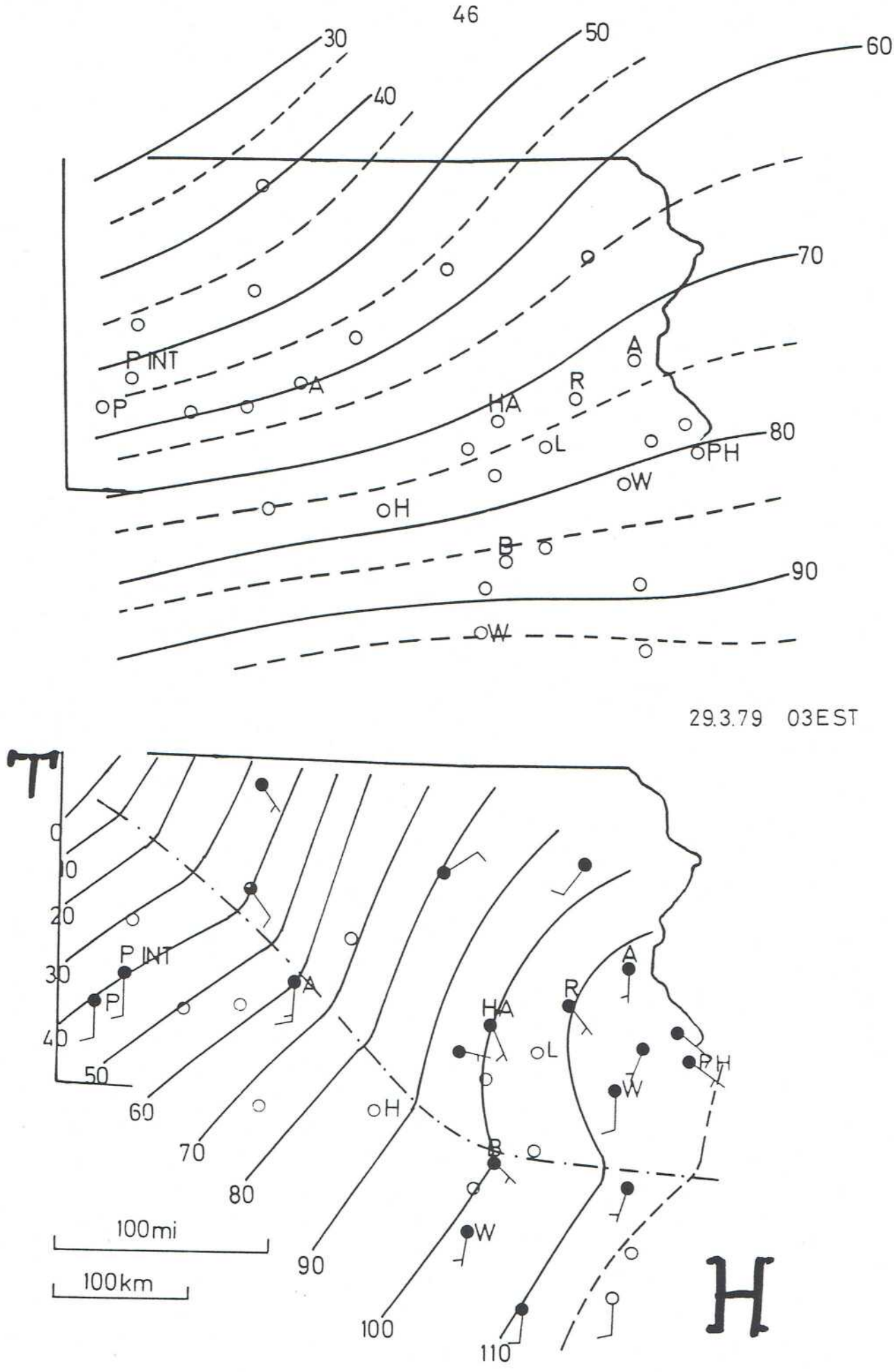

Fig. 5.15: *850 mb and surface maps for indicated date. See fig. 5.4*

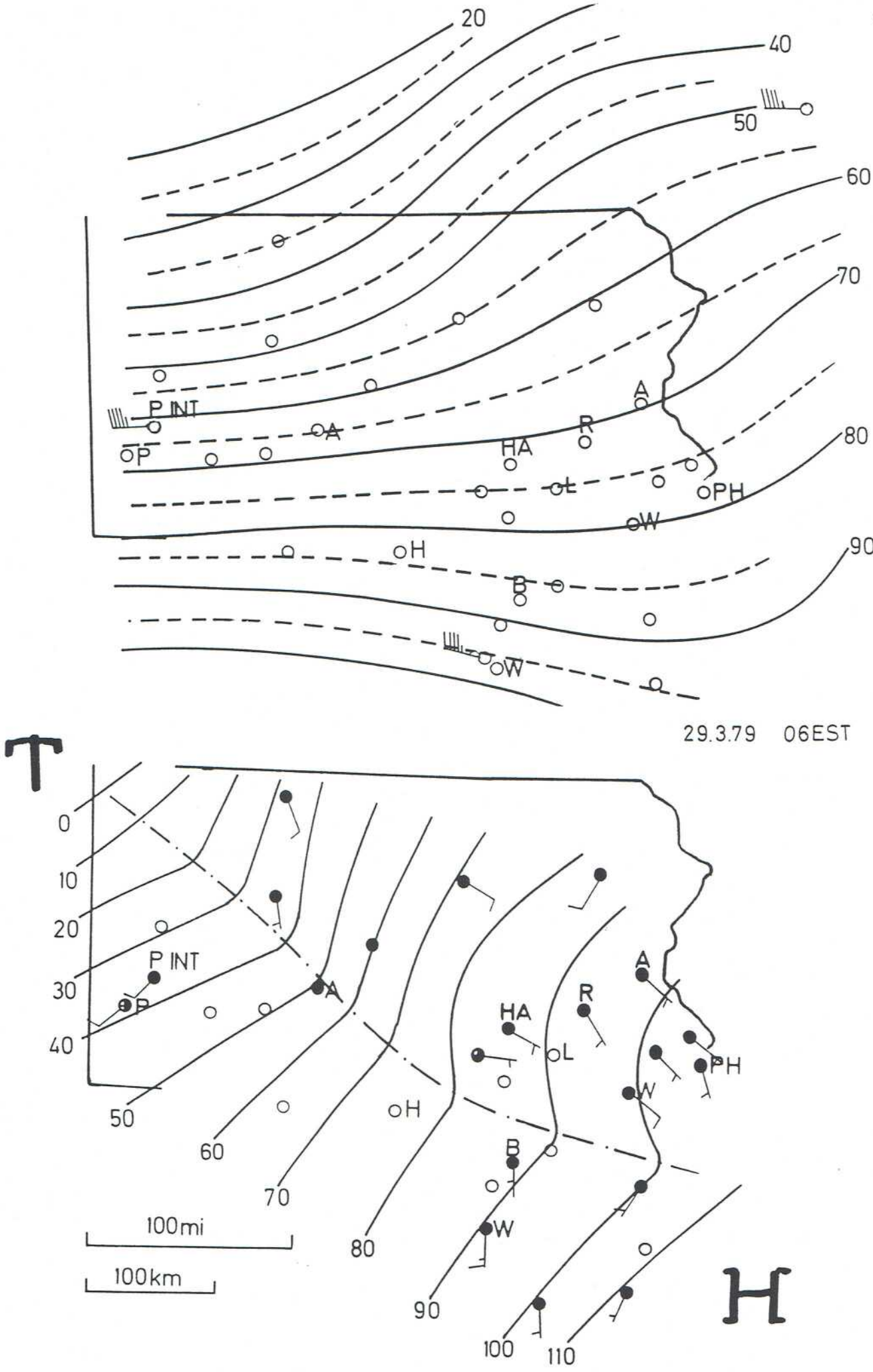

Fig. 5.16: *850 mb and surface maps for indicated date. See fig. 5.4*

By that time, the picture gets complicated by the approach of a first warm front. In the earlier analysis (part I, fig. 2.6 a), the first warm front is still located further back towards the SW by 29/07. Surface temperatures do not clearly support the frontal zone to be as far advanced as shown on figs. 5.15 b and 5.16 b. However, there is a definite cyclonic wind shift in agreement with the station pressures evident on these surface maps. This feature may be a reflection of the warm frontal position at 850 mb (part I, fig. 2.5), which, indeed, stretches right across the area by 29/07. The pressure field, hydrostatically, will reflect this elevated temperature structure and leave the pertinent signal in the surface pressure observations, unimpressed by any shallow near-surface feature.

6. Numerical Model Results

A numerical model, like any model, is a simplification of the complexities of air flows.
In general, it should be more realistic than a shallow-water model (see the next chapter 7), but in practice a limited-area numerical model can be severely limited by its structure, inability to take synoptic constraints or slope wind circulations into account, inability to accomodate lateral boundary conditions (in our case, they are unknown anyway) and other deficiencies to be listed below.

This does not mean that we cannot learn from a model, only that we must not overinterpret the results.

Save for tests, essentially two cases were run with the FITNAH model, operated by AMBIMET in Munich, Germany (Dr. Dieter Heimann). The model's most stringent limitations in its present form are probably that one can really only prescribe one wind vector (surface wind or geostrophic wind, both related to each other by the usual frictional empirical law), and that only the stationary solution is being computed, with the meteorology "kept frozen". Nonstationary features cannot be described. An arbitrary relief of hills and valleys can be used as the lower boundary, in our case essentially the relief shown in fig. 5.1.

Once the stationary flow field including the field of turbulent kinetic energy has been computed, 15000 "Lagrangian" particles are simultaneously started at the vent stack and traced through the fluid, each being transported at the mean three-dimensional velocity plus a random turbulent fluctuation, prescribed according to a suitably parameterized Markov model. The number of particles and their residing time in each of many accounting grid boxes are being evaluated, from which normalized concentrations X/Q (s/m^{-3}, see chapter 8.5) may be derived. Accounting can also be done in the "puff mode" (instantaneous release), in which case the resulting "concentration factor" has the dimension m^{-3}, yielding, e. g., Ci/m^3 when multiplied by the total release Q^* (Ci).

Horizontal grid: 45 x 49 grid points, spacing Δx = 800 m
Vertical grid: Variable resolution, 16 levels.

Case 1: March 28, 1979, 17.30 E.S.T.
Surface wind ≈ 4 m/s from the south (180 °)
Geostrophic wind ≈ 17 m/s from 212 °
Lowest 1.2 km nearly well-mixed, extremely stable above.

The flow field shows only small deviations from the southerly direction in this case, as the Blue Mountain Range is outside our domain of computation. Due to forced flow over the hills, vertical motions reach up to more than half a m/s. The plume at the surface stretches away almost straight towards the north.
Dispersion factors X/Q are close to 10^{-6} sm^{-3} even at a downstream distance of 15 km. Compare the values quoted in chapter 8.

Case 2: March 28, 1979, 07 E.S.T.
Surface wind at less than 1 m/s from the east (90 °)
Geostrophic wind ≈ 1.5 m/s from 120 °
Lowest 1.2 km fairly stable, extremely stable above.

This flow, small wonder, shows the air being deflected strongly around the hills (fig. 6.1). Note that this figure shows the wind at 10 m above ground level, such that the tops of most hills reach into the upper east-southeasterly current. It would be more impressive to see the wind at a fixed mean sea level, close to the actual plane of flow, with the topography blocked out where it reaches higher up. Such a figure is not available.

Particles travel very slowly in this almost stagnating flow. As the release has been assumed at 70 m a. g., the cloud of particles moves with the eastsoutheasterly "upper" wind, straddling the first larger hill it encounters. The particles tend to stay and recirculate in the area. Therefore, accounting for this case is done in the puff mode, with a maximum resulting "concentration factor" in any surface box of ≈ 15 x 10^{-9} m^{-3}. Tentatively converting a plume segment 8 minutes long into a puff (Q^* = Q x 500 s), the "dispersion factor" X/Q (see chapter 8.5) would come out to be ≈ 7.5 x 10^{-6} sm^{-3}. Remember, however, that this value is the average over an accounting box with dimensions 800 m x 800 m x 10 m. I refer to the pertinent discussion in my part I, chapters 5 and 7. Averaging over a relatively large volume smears out local concentration maxima. My estimate for the Lewisberry area (test case) is X/Q ≈ 10^{-5} sm^{-3}, which is only slightly higher than the abovequoted maximum. Local maxima on a scale smaller than 800 m x 800 m could be considerably higher yet.